

COMPUTATION OF A COMBINED SPHERICAL-ELASTIC AND VISCOUS-HALF-SPACE EARTH MODEL FOR ICE SHEET SIMULATION

ED BUELER¹, CRAIG S. LINGLE², AND JED A. KALLEN-BROWN¹

ABSTRACT. This report starts by describing the continuum model used by Lingle & Clark (1985) to approximate the deformation of the earth under changing ice sheet and ocean loads. That source considers a single ice stream, but we apply their underlying model to continent-scale ice sheet simulation. Their model combines Farrell’s (1972) elastic spherical earth with a viscous half-space overlain by an elastic plate lithosphere. The latter half-space model is derivable from calculations by Cathles (1975). For the elastic spherical earth we use Farrell’s tabulated Green’s function, as do Lingle & Clark. For the half-space model, however, we propose and implement a significantly faster numerical strategy, a spectral collocation method (Trefethen 2000) based directly on the Fast Fourier Transform. To verify this method we compare to an integral formula for a disc load. To compare earth models we build an accumulation history from a growing similarity solution from (Bueler, et al. 2005) and and simulate the coupled (ice flow)-(earth deformation) system. In the case of simple isostasy the exact solution to this system is known. We demonstrate that the magnitudes of numerical errors made in approximating the ice-earth system are significantly smaller than pairwise differences between several earth models, namely, simple isostasy, the current standard model used in ice sheet simulation (Greve 2001, Hagdorn 2003, Zweck & Huybrechts 2005), and the Lingle & Clark model. Therefore further efforts to validate different earth models used in ice sheet simulations are, not surprisingly, worthwhile.

1. TWO LINEAR EARTH MODELS AND THEIR GREEN’S FUNCTIONS

Lingle & Clark (1985) use as their fundamental tools the Green’s functions of two different linear earth models. The Green’s functions for these models are convolved with the load to compute (vertical) displacements of the earth’s surface. One finds an elastic displacement u^E and a viscous displacement u^V given a current load and a load history, respectively, as we will explain. The total displacement is then the sum $u = u^E + u^V$ at any time. That is, the two linear models are superposed.

The partial differential equations (PDEs) behind these Green’s functions are linear. In this report we state these PDEs, which is, in the case of the second model, a nontrivial accomplishment (see section 3). We then approximately solve these PDEs in a demonstrably efficient manner. First, however, we describe the two models and their sources in the literature.

DRAFT JULY 3, 2021.

¹Dept. of Mathematics and Statistics, Univ. of Alaska, Fairbanks AK 99775-6660. Email ffe1b@uaf.edu.

²Geophysical Institute, Univ. of Alaska, Fairbanks AK 99775-6660.

An elastic, self-gravitating spherical earth. The main equations of this model are labeled (27) in (Farrell 1972):

$$\begin{aligned}\nabla \cdot \boldsymbol{\tau} - \nabla(\rho g \mathbf{s} \cdot \mathbf{e}_r) - \rho \nabla \phi + g \nabla \cdot (\rho \mathbf{s}) \mathbf{e}_r + \rho \ddot{\mathbf{s}} &= 0, \\ \nabla^2 \phi &= -4\pi G \nabla \cdot (\rho \mathbf{s})\end{aligned}$$

Here $\rho = \rho(r)$ is the density of the earth. (We restrict to only radial dependence because the densities used by (Farrell 1972) are for “stratified” earths.) Also, g is the acceleration of gravity, $\boldsymbol{\tau}$ is the full stress tensor, and \mathbf{s} is the displacement vector field (i.e. the strain field) which we seek. The gravitational potential ϕ is described below. Note that $\dot{\mathbf{s}} = \mathbf{u}$ is the velocity field and that $\ddot{\mathbf{s}}$ is just the acceleration.

The first equation comes from formally linearizing the equation of conservation of momentum. The second equation is for the gravitational potential. The field ϕ is the *additional* gravitational potential “on top of” that caused by the undeformed earth and also additional to the potential of any masses outside the earth (including the load). In Farrell’s words “. . . ϕ is the perturbation in the ambient gravitational potential ϕ_1 plus the potential of any externally applied gravitational force field ϕ_2 .”

Actually, equation (27) in (Farrell 1972) has “ $-\omega^2 \rho \mathbf{s}$ ” where we have “ $\rho \ddot{\mathbf{s}}$ ” because Farrell only states the Fourier-transformed-in-time equations. We will only be interested in the $\ddot{\mathbf{s}} = 0$, equivalently $\omega = 0$ case, however, because we are interested in phenomena on the scale of years or centuries, unlike Farrell who was interested in tides.

Consider point forces or disk loads at the surface. For such loads it is natural to use spherical coordinates (r, θ, φ) where the z -axis is along the line between the center of the earth and the center of the load. Here θ is the angle between the position vector and the z -axis (i.e. the colatitude) and φ is the longitude. The load is at the “north pole.”

For the resulting stratified problem we seek the components of \mathbf{s} which do not vanish, namely s_r and s_θ in $\mathbf{s} = s_r(r, \theta) \mathbf{e}_r + s_\theta(r, \theta) \mathbf{e}_\theta$. By symmetry the “toroidal” component of the strain, s_φ , vanishes everywhere. Also we seek the potential $\phi = \phi(r, \theta)$. The functions s_r, s_θ, ϕ are expanded in spherical harmonics with radially-dependent coefficients; see equation (28) in (Farrell 1972). The radially-dependent coefficients, for each degree in the expansion, solve a system of ODEs in the radial coordinate r . Using a radially-dependent density for the earth these can be solved numerically by standard ODE means. Note that (Farrell 1972) and (Lingle & Clark 1985) choose the “Gutenberg-Bullen A” model. For the Green’s function corresponding to a point load, Farrell has done this using a Runge-Kutta method, and we accept and use the tabulated result.

Following (Lingle & Clark 1985) we are only interested in the vertical displacement of the surface of the earth, and therefore the vertical displacement $u(\theta)$ corresponding to a point load is the Green’s function we seek. In terms of the spherical harmonics expansion the relevant equation is equation (37) in (Farrell 1972). Farrell computes this Green’s function and reports its values at particular distances in his table A3. Table 1 in (Lingle & Clark 1985) also reports this data. One must be clear on normalization so a plot is in order here. Let $G^E(r)$ be the vertical displacement caused by a 1 kg mass at the north pole and evaluated at a distance r along the surface of the earth. (The coordinate r here has a different meaning from the spherical coordinate of the same name. Specifically, the new variable $r = a\theta$ if a is the radius of the earth and θ is the spherical coordinate, the radian colatitude.) Figure 1

shows $G^E(r)$. There is a $1/r$ singularity to this elastic Green's function, in contrast to the Green's function for the flat, viscous model which follows.

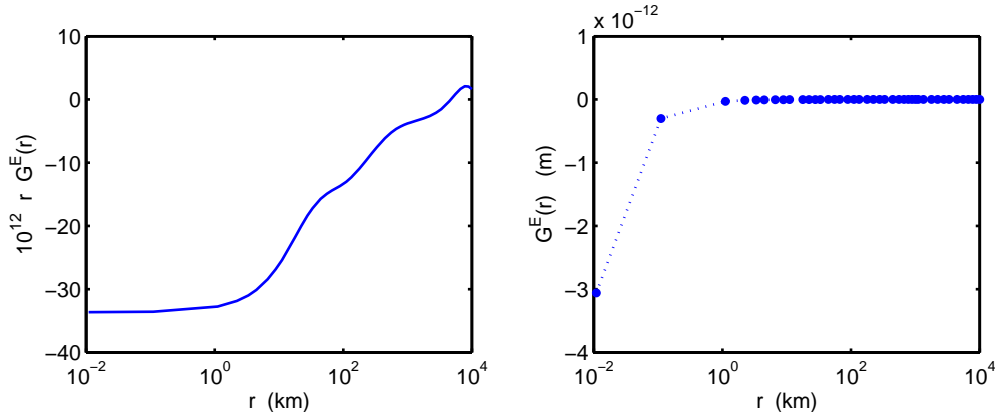


FIGURE 1. Two views of the vertical surface displacement Green's function $G^E(r)$ for the elastic spherical self-gravitating earth model (Farrell 1972). Here r is the distance along the surface of the earth from the point of application of the load. Left: the smooth normalized form $rG^E(r)$. Right: the same data without normalization, suggesting the actual $1/r$ singularity. Note log scale on the horizontal axes.

This elastic Green's function is used as described in equation (20) in (Lingle & Clark 1985) and as follows. Suppose we seek the vertical displacement $u^E = u^E(x, y, t)$, caused by elastic deformation of the spherical earth. Suppose the load at time t is given by the function $\Psi(x, y, t)$, with units of mass per unit area. Then

$$u^E(x, y, t) = \iint_R G^E(|\mathbf{r} - \mathbf{r}'|) \Psi(x', y', t) dx' dy', \quad (1)$$

where we define $|\mathbf{r} - \mathbf{r}'|^2 = (x - x')^2 + (y - y')^2$, of course, and where R denotes a map-plane region containing the load. Clearly the displacement u^E depends on time only through the changing load; elastic changes are instantaneous.

In using (1) we necessarily project the earth's geoid into a fixed plane. This projection means our results are limited to an appropriately small region of the earth's surface. We do integral (1) numerically as explained in section 2.

A viscous, flat earth overlain by an elastic plate. Next we describe the time-dependent Green's function for a model which comes from (Cathles 1975). The PDE actually solved by this Green's function is given in section 3.

Cathles' sub-subsection III.A.2.e, pp. 50–55, describes a viscous half-space asthenosphere overlain by an elastic plate lithosphere. An important point about this model, which partly explains the superposition " $u^E + u^V$ " used by (Lingle & Clark 1985), is that the elastic plate lithosphere used here deflects but does not compress in the vertical. Therefore all vertical motion in this model is really asthenosphere motion, though the elastic plate spreads the influence of any load. The just-described spherical elastic earth exhibits elastic compression, however.

Unfortunately, all we are given in (Cathles 1975) are the Hankel transforms of the actual equations. Roughly speaking, from (Cathles 1975) we use equation (III-35) along with the definitions of “ α ” and “ D ” contained in the footnote on page 52 (Lingle 2005, personal communication). Precisely speaking, however, our source is (Lingle & Clark 1985), from which we use equations (4), (7), and (8)–(14). We will also use the particular choices of layer thickness, viscosity, and flexural rigidity for the “two-layer” model from that source. We now repeat some equations from (Lingle & Clark 1985) as needed for clarity.

Let $u^V(r, t)$ be the vertical displacement of the surface supposing a point load at the origin $r = 0$ applied at time $t = 0$ and held. Consider the Hankel transform of this function

$$\bar{u}^V(\kappa, t) = \int_0^\infty u^V(r, t) J_0(\kappa r) r dr,$$

where J_0 is the Bessel function of zero order (see Appendix A). The Hankel transform is self-inverse, so u^V can be recovered from \bar{u}^V by the same integral.

The half-space model hypothesizes (Lingle & Clark 1985) that \bar{u}^V solves the equation

$$\frac{\partial \bar{u}^V}{\partial t} + \frac{\rho_r g \alpha(\kappa)}{2\eta\kappa} \bar{u}^V = \frac{\bar{\sigma}_{zz}(\kappa, t)}{2\eta\kappa} \quad (2)$$

where

$$\alpha(\kappa) = 1 + \frac{D\kappa^4}{\rho_r g} \quad \text{and} \quad D = \frac{ET^3}{12(1 - \nu^2)}.$$

We denote by $\bar{\sigma}_{zz}$ the Hankel transform of the normal stress from a point load applied at the origin

$$\bar{\sigma}_{zz}(\kappa, t) = -\frac{g}{2\pi} H(t), \quad (3)$$

in units of N m^{-2} , corresponding to a point mass of 1 kg. Here $H(t)$ is the Heaviside function ($H(t) = 1$ for $t \geq 0$ and $H(t) = 0$ otherwise). Note $\bar{\sigma}_{zz}(\kappa, t)$ is the Hankel transform of $\sigma_{zz}(r, t) = -g\delta_0(r)H(t)$ where $\delta_0(r)$ is the Dirac delta function at the origin which acts on functions on the plane.¹ The initial condition to (2) is the condition of zero displacement

$$\bar{u}^V(\kappa, 0) = 0.$$

That is, $\bar{u}^V(\kappa, t)$ is the Hankel transform of the Heaviside Green’s function of an as yet unstated PDE of which (2) is the Hankel-transformed version; see section 3 for clarification of this description.

Poisson’s ratio and Young’s modulus for the elastic plate lithosphere are assumed to be $\nu = 0.5$ and $E = 6.6 \times 10^{10} \text{ M/m}^2$, respectively. The lithosphere thickness T is assumed to be 88 km. The resulting flexural rigidity is $D = 5.0 \times 10^{24} \text{ N m}$. The density and viscosity of the fluid in the underlying half-space are assumed to be $\rho_r = 3300 \text{ kg/m}^3$ and $\eta = 10^{21} \text{ Pa s}$, respectively.

Equation (2) is an uncoupled set of linear first order ODEs in time. That is, the spatial Hankel transform has done its job and turned a PDE into a solvable system. Let² $\beta(\kappa) = \rho_r g \alpha(\kappa) = \rho_r g + D\kappa^4$. The solution of (2) and (3) is

$$\bar{u}^V(\kappa, t) = -\frac{g}{2\pi\beta(\kappa)} \left(1 - \exp[-\beta(\kappa)t/(2\eta\kappa)] \right) \quad (4)$$

¹See Appendix A and especially equation (42) for the defining property of $\delta_0(r)$.

²Use of β instead of α represents an admittedly minor simplification of the notation in (Lingle & Clark 1985).

for $t > 0$ and $\bar{u}^V(\kappa, t) = 0$ for $t \leq 0$. Because of the self-inverse property of the Hankel transform, we have the following integral formula for the Green's function:

$$G^V(r, t) = u^V(r, t) = -\frac{g}{2\pi} \int_0^\infty \beta(\kappa)^{-1} \left(1 - \exp[-\beta(\kappa)t/(2\eta\kappa)]\right) J_0(r\kappa) \kappa d\kappa, \quad (5)$$

for $t > 0$ and $G^V(r, t) = 0$ for $t < 0$. This formula is equation (14) in (Lingle & Clark 1985). Note G^V has units m kg^{-1} ; see formula (6) below.

As far as we know the integral (5) must be computed numerically. Furthermore there seems to be no one-dimensional procedure analogous to the Fast Fourier Transform (FFT) (Bracewell 1978) to do the job quickly. Our strategy for the similar disc load integral (Appendix B) is to break up the oscillatory integral into more than 100 subintervals and call an adaptive quadrature routine for each subinterval. This strategy is essentially the same as that described on page 1104 of (Lingle & Clark 1985) for (5).

Unlike the elastic case, the Green's function G^V is time-dependent. A graph of G^V for several t values is shown in figure 2. The viscous behavior is clear, as is the role of the elastic plate lithosphere in removing any singularity at $r = 0$. Note that the peripheral bulge develops only at large times; compare the "standard" model in section 4.

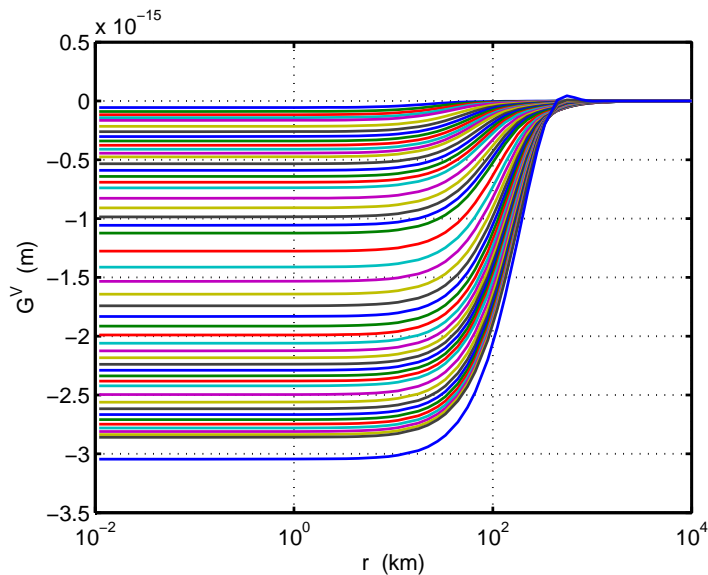


FIGURE 2. Green's function $G^V(r, t)$ for the viscous flat earth model. The curves are from times given in table 1 in (Lingle & Clark 1985); compare figure 5(a) there. The top curve is at $t = 20$ years and the bottom at 10^5 years. Not log scale on the horizontal axis.

A method for using G^V to compute the response to arbitrary load is described in equations (19) and (22) in (Lingle & Clark 1985), and as follows. Suppose there is a load function $\Psi(x, y, t)$, with units of mass per unit area, on some region R of our map-plane. The time rate of change of this load function, or, equivalently, the incremental changes in this load function, are what we sum using G^V to find the general (viscous) displacement $u^V = u^V(x, y, t)$ of the surface. In fact, let

$$\lambda(x, y, t) = \frac{\partial \Psi}{\partial t}(x, y, t).$$

Then Lingle & Clark assert (with a heuristic motivation; pp. 1105–1106) that:

$$u^V(x, y, t) = \int_{-\infty}^t \iint_R G^V(|\mathbf{r} - \mathbf{r}'|, t - t') \lambda(x', y', t') dx' dy' dt'. \quad (6)$$

Note that the right side of (6) has units of length because G^V has units m kg^{-1} , as noted, and λ has units $\text{kg m}^{-2} \text{s}^{-1}$.

Lingle & Clark (1985) describe the function λ discretely, thereby incorporating an approximation of the rate of change of the load. Some such approximation is essential in practice, of course. They suppose a fixed sequence of past times $\{t_i\}$ and define

$$\Lambda(x, y, t_i) = \int_{t_{i-1}}^{t_i} \lambda(x, y, t) dt = \Psi(x, y, t_i) - \Psi(x, y, t_{i-1}),$$

so

$$u^V(x, y, t) \approx \sum_i \iint_R G^V(|\mathbf{r} - \mathbf{r}'|, t - t_i) \Lambda(x', y', t_i) dx' dy'; \quad (7)$$

compare equations (16) and (17) in (Lingle & Clark 1985).

2. THE LOAD RESPONSE MATRIX METHOD

Suppose now that the map-plane region R is divided into a grid of rectangular elements of area $\Delta x \Delta y$. Concretely, suppose $R = [-L_x, L_x] \times [-L_y, L_y]$ is a rectangular region, suppose N_x, N_y are positive integers, and let $\Delta x = (2L_x)/N_x$, $\Delta y = (2L_y)/N_y$. Center each element at $(x_j, y_k) = (-L_x + (j - 1/2)\Delta x, -L_y + (k - 1/2)\Delta y)$. There are $M = N_x N_y$ elements, each denoted by a pair (j, k) for $1 \leq j \leq N_x$, $1 \leq k \leq N_y$.

We define the *elastic load response matrix* (LRM) $\{\Gamma_{(jk)(mn)}\}$, $j, m = 1, \dots, N_x$, $k, n = 1, \dots, N_y$, as the vertical displacement of element (j, k) caused by a unit change in ice thickness within element (m, n) ; compare (Lingle & Clark 1985) page 1106. This displacement is assumed constant within element (j, k) . (As it stands, this description applies only to the elastic spherical model in the previous section. Slightly different conventions apply to the LRM for the viscous earth model; see below.)

We compute $\{\Gamma_{(jk)(mn)}\}$ by integrating over element (m, n) :

$$\Gamma_{(jk)(mn)} = \rho_i \int_{y_n - \Delta y/2}^{y_n + \Delta y/2} \int_{x_m - \Delta x/2}^{x_m + \Delta x/2} G^E \left(\sqrt{(x_j - x)^2 + (y_k - y)^2} \right) dx dy, \quad (8)$$

where $\rho_i = 910 \text{ kg m}^{-3}$ is the density of ice. Note that the load per unit area (i.e. Ψ in the last section) for a unit (i.e. one meter) change in ice thickness on a rectangle of area $\Delta x \Delta y$ is

$$\Psi = \frac{\text{mass}}{\text{area}} = \frac{\rho_i (1 \cdot \Delta x \cdot \Delta y)}{\Delta x \Delta y} = \rho_i.$$

That is, equation (8) is a special case of equation (1).

The matrix $\{\Gamma_{(jk)(mn)}\}$ is $M \times M$ if we linearly order all elements; alternatively Γ could be regarded as a “4-tensor” with indices j, k, m, n . There are symmetries in this object, and we may exploit them to compute roughly $(2N_x)(2N_y) = 4M$ integrals (8) rather than doing

an integral for each of the M^2 entries of $\Gamma_{(jk)(mn)}$. In fact, if we change variables in (8) by $x = x_m - \xi$, $y = y_n - \zeta$ then we get

$$\Gamma_{(jk)(mn)} = \rho_i \int_{-\Delta y/2}^{\Delta y/2} \int_{-\Delta x/2}^{\Delta x/2} G^E \left(\sqrt{((j-m)\Delta x - \xi)^2 + ((k-n)\Delta y - \zeta)^2} \right) d\xi d\zeta.$$

Let

$$I^E(p, q) = \int_{-\Delta y/2}^{\Delta y/2} \int_{-\Delta x/2}^{\Delta x/2} G^E \left(\sqrt{(p\Delta x - \xi)^2 + (q\Delta y - \zeta)^2} \right) d\xi d\zeta \quad (9)$$

for $-N_x + 1 \leq p \leq N_x - 1$, $-N_y + 1 \leq q \leq N_y - 1$. Then

$$\Gamma_{(jk)(mn)} = \rho_i I^E(j - m, k - n).$$

We need only compute the $(2N_x - 1)(2N_y - 1)$ entries of I^E . Integral (9) can be done numerically, getting values for the integrand $G^E(\dots)$ by interpolation between the values computed by Farrell.

Now let $H_{(mn)}$ be the average value of the ice thickness $H(x, y, t)$ over element (m, n) . Following Lingle & Clark we call $\{H_{(mn)}\}_{m,n=1}^{N_x, N_y}$ the *load vector*. (Technically it is a *thickness* vector, actually; if the load is actually liquid water one computes the equivalent thickness to give values $H_{(mn)}$.) Integral (1), which gives the elastic displacement from the load, is approximated by

$$u^E(x_j, y_k, t) \approx \sum_{m=1}^{N_x} \sum_{n=1}^{N_y} \Gamma_{(jk)(mn)} H_{(mn)} = \sum_{m=1}^{N_x} \sum_{n=1}^{N_y} \rho_i I^E(j - m, k - n) H_{(mn)}. \quad (10)$$

Note that as a straightforward matrix-vector product, (10) requires $M = N_x N_y$ scalar multiplications to compute the elastic displacement in the (j, k) element, and thus M^2 multiplications are required to update u^E at each timestep.

A comparable LRM approximation applies to the viscous model. Let $\{\Delta t_i\}_{i=1}^{N_t}$ be a decreasing sequence of N_t positive times. These values are time intervals before the present time; table 3 in (Lingle & Clark 1985) gives a list of 26 values. Let $\Phi_{(jk)(mn)}^i$ be the displacement in element (j, k) caused by a change in ice thickness of 1 meter in element (m, n) at time Δt_i before the current time. From (7),

$$\Phi_{(jk)(mn)}^i = \rho_i \int_{y_n - \Delta y/2}^{y_n + \Delta y/2} \int_{x_m - \Delta x/2}^{x_m + \Delta x/2} G^V \left(\sqrt{(x_j - x)^2 + (y_k - y)^2}, \Delta t_i \right) dx dy. \quad (11)$$

Compare to equation (8) for the elastic case. Let $\Lambda_{(mn)}^i$ be the average value of the change in ice thickness $H(x, y, t - \Delta t_{i+1}) - H(x, y, t - \Delta t_i)$ over element (m, n) . Then

$$u^V(x_j, y_k, t) \approx \sum_{i=1}^{N_t} \sum_{m=1}^{N_x} \sum_{n=1}^{N_y} \Phi_{(jk)(mn)}^i \Lambda_{(mn)}^i. \quad (12)$$

As it stands, matrix-vector product (12) requires $N_t M = N_t N_x N_y$ scalar multiplications to compute the (j, k) element, thus $N_t M^2$ multiplications to update u^V .

As noted at the beginning, we superpose the results from these elastic and viscous LRM approximations:

$$u(x_j, y_k, t) \approx \sum_{m,n} \Gamma_{(jk)(mn)} H_{(mn)} + \sum_i \sum_{m,n} \Phi_{(jk)(mn)}^i \Lambda_{(mn)}^i. \quad (13)$$

Compare equation (25) in (Lingle & Clark 1985).

We are concerned with computability in reasonable time. By using (13) to update every element at a given simulation timestep requires

$$(1 + N_t) \cdot M \cdot M = O(N_t M^2) = O(N_t N_x^2 N_y^2) \quad (14)$$

scalar multiplications. Lingle & Clark (1985) used $M = 38$, as this was the number of 50 km long elements into which the flowline—a single ice stream and included ocean—was divided. For Antarctica simulations with Δx on the order of 50 km or so, the minimum reasonable number of elements is $N_x = N_y$ at least 80 so $M \geq 6400$. Note that N_t is roughly independent of the nature of the problem, as long as it involves large amounts of polar ice. Thus by (14) an Antarctica problem is roughly a factor of

$$(6400^2)/(38^2) \approx 3 \times 10^4$$

times more expensive in computation than the problem addressed in (Lingle & Clark 1985) if one directly implements the load response matrix method using matrix multiplication. Such poor scaling of this numerical method clearly represents a danger when using it in an ice sheet simulation.

A major speedup is possible if one uses the convolution sum form of the multiplication, as in equation (10) when I^E is used. (An obvious corresponding construction of a function $I^V(p, q, t)$ is needed to make the viscous LRM computations above into convolutions. As it turns out, we will not need that construction.) Convolutions sums can be quickly computed by the Fast Fourier Transform (FFT). Using standard estimates on the time for the FFT (Briggs & Henson 1995), we can reduce the time to

$$(1 + N_t) \cdot M \log M = O(N_t N_x N_y \log N_x \log N_y). \quad (15)$$

Compare this with (14) above. One must still, however, precompute the LRMs, which turns out to be more expensive than solving the whole problem (over quite long time scales) if one uses the method of the next section. In addition, the method of the next section eliminates a factor of N_t work in a time-dependent simulation. The method of the next section also significantly reduces memory usage.

3. THE STRAIGHT-FROM-THE-PDE METHOD

Derivation. We now reverse engineer some of the Green’s function and Hankel transform “thinking” in the previous sections. We recover the PDE underlying the half-space viscous model (2). Actually, the resulting equation is not, technically, a *partial differential* equation. It is a linear pseudo-differential equation easily understood through the Fourier transform. We have already computed solutions of this PDE by the Hankel transform, by the indirect method of Green’s functions. In any case, analyzing the new PDE will lead to a much more efficient method for computing deformation in the half-space model. We must still use, for now, the Green’s function and LRM for the *elastic* response computed from the Farrell (1972) spherical earth model; we will implement the convolution sum (10) by the FFT.

Returning to equation (2), we apply the inverse Hankel transform. In fact (2) is equivalent to

$$\frac{\partial}{\partial t} (2\eta\kappa\bar{u}) + \rho_r g \bar{u} + D\kappa^4 \bar{u} = \bar{\sigma}_{zz}, \quad (16)$$

denoting $u = u^V$ for the rest of this section, and with the Hankel transform $\bar{u} = \bar{u}^V$. As shown in Appendix A, the multiplication by κ^1 and κ^4 which appear in equation (16) can be

regarded as the action of operators which are powers of the Laplacian operator. In particular,

$$\Delta = -\nabla^2 = -\left(\frac{\partial^2}{\partial x^2} + \frac{\partial^2}{\partial y^2}\right)$$

acts on the Hankel transform of a radial function $f = f(r)$ by multiplication by κ^2 :

$$\overline{\Delta f}(\kappa) = \kappa^2 \bar{f}(\kappa).$$

In fact Δ is the *positive* Laplacian as we see it is equivalent to multiplication by a nonnegative factor. The inverse Hankel transform of (16) is

$$\frac{\partial}{\partial t} \left(2\eta \Delta^{1/2} u\right) + \rho_r g u + D \Delta^2 u = \sigma_{zz} \quad (17)$$

for $u(r, t)$. Equation (17) is the “underlying PDE” for equation (2). The symbol Δ^2 stands for the standard biharmonic fourth-order differential operator

$$\Delta^2 f = f_{xxxx} + 2f_{xxyy} + f_{yyyy}$$

(Sneddon 1951, section 20). The operator $\Delta^{1/2}$ is not a differential operator but is definable via the Fourier transform in general; see Appendix A. One can also write equation (17) as

$$\frac{\partial}{\partial t} (2\eta |\nabla| u) + \rho_r g u + D \nabla^4 u = \sigma_{zz}$$

if the meaning $|\nabla| = \sqrt{-\nabla^2}$ is understood.

To confirm the equivalence of (2) and (17) the reader may verify that the Green’s function $G^V(r, t)$ defined by (5) satisfies

$$\frac{\partial}{\partial t} \left(2\eta \Delta^{1/2} G^V\right) + \rho_r g G^V + D \Delta^2 G^V = -g \delta_0(r) H(t).$$

From now on we remove the assumption of radial load, and suppose equation (17) applies for any load $\sigma_{zz}(x, y, t)$. The solution $u(x, y, t)$ is a function of three variables; it is no longer radial.

Note that the equilibrium of (17) is a standard rigid plate equation with a bouyant restoring force:

$$D \nabla^4 u = \sigma_{zz} - \rho_r g u. \quad (18)$$

For example, this is equation (8.7.3) in (van der Veen 1999).

The interesting part of (17) is the time-derivative term. This term accounts for viscous flow within the mantle. It is not completely clear to the author at the present time why the particular power $\Delta^{1/2}$ appears or why it represents the correct diffusive behavior. The units in equation (17) are consistent only with the 1/2 power of the Laplacian, however.

The Fourier transform of (17) is worth noting, because, as in the special case of a radial load wherein we may use the Hankel transform, we can write the solution as an integral. Namely, if $\tilde{u}(\xi, \zeta, t)$ is the two-variable, spatial Fourier transform of $u(x, y, t)$,

$$\tilde{u}(\xi, \zeta, t) = \frac{1}{2\pi} \int_{-\infty}^{\infty} \int_{-\infty}^{\infty} u(x, y, t) e^{-i(x\xi + y\zeta)} dx dy,$$

then (17) is equivalent to

$$\frac{\partial}{\partial t} \left(2\eta (\xi^2 + \zeta^2)^{1/2} \tilde{u}\right) + \rho_r g \tilde{u} + D (\xi^2 + \zeta^2)^2 \tilde{u} = \tilde{\sigma}_{zz}. \quad (19)$$

As with equation (2), this is a decoupled system of first order ODEs in time. Using initial condition $u(x, y, t_0)$ the solution is

$$\begin{aligned} \tilde{u}(\xi, \zeta, t) = & \int_{t_0}^t \frac{\exp[-\beta(\xi, \zeta)(t-s)/(2\eta(\xi^2 + \zeta^2)^{1/2})]}{2\eta(\xi^2 + \zeta^2)^{1/2}} \tilde{\sigma}_{zz}(\xi, \zeta, s) ds \\ & + \exp\left[-\beta(\xi, \zeta)(t-t_0)/(2\eta(\xi^2 + \zeta^2)^{1/2})\right] \tilde{u}(\xi, \zeta, t_0) \end{aligned} \quad (20)$$

where $\beta(\xi, \zeta) = \rho_r g + D(\xi^2 + \zeta^2)^2$. To find u itself one needs to do the inverse Fourier transform, and this could, potentially, be done by the FFT. In fact we will compute more directly with (17), and we will avoid the integral over time in (20).

Appendix C illustrates the relationship of formula (20) to the Hankel transform formulas in section 1.

Implementation. We now treat PDE (17) numerically by discretizing using a finite difference method in time and then computing the action of $\Delta^{1/2}$ and Δ^2 using the FFT. Our method produces a “whole new ball game” numerically relative to integral formulations (the LRM method). The resulting new method can be called a *Fourier spectral collocation* method (Trefethen 2000).

We discretize in time by the trapezoid rule—analogueous to the Crank-Nicolson method for the heat equation (Morton & Mayers 1994)—and get an unconditionally stable $O(\Delta t^2)$ method for equation (17). In particular, let $t_n = n\Delta t$ for $n = 0, 1, 2, 3, \dots$ and let $U^n(x, y)$ be our approximation of $u(x, y, t_n)$. Equation (17) is approximated by

$$\begin{aligned} \left(2\eta \Delta^{1/2} U^{n+1}\right) + \frac{\Delta t}{2}(\rho_r g U^{n+1} + D\Delta^2 U^{n+1}) \\ = \left(2\eta \Delta^{1/2} U^n\right) - \frac{\Delta t}{2}(\rho_r g U^n + D\Delta^2 U^n) + \Delta t \sigma_{zz}(x, y, t^*). \end{aligned} \quad (21)$$

Here either $\sigma_{zz}(x, y, t^*) = \sigma_{zz}(x, y, (n + 1/2)\Delta t)$ if the load is known at the time $t^* = (n + 1/2)\Delta t$ or $\sigma_{zz}(x, y, t^*) = \frac{1}{2}(\sigma_{zz}(x, y, t_n) + \sigma_{zz}(x, y, t_{n+1}))$ if the load is only known at the times t_n, t_{n+1} ; both choices preserve $O(\Delta t^2)$ accuracy and unconditional stability.

Equation (17) needs boundary conditions and, in fact, we assume $u(x, y, t) \rightarrow 0$, and similarly for a sufficient number of its derivatives, as $(x, y) \rightarrow \infty$. We also assume that the support of the continuous function $\sigma_{zz}(x, y, t)$ is bounded for each t . That is, we assume there is a zero boundary condition at infinity for the rigid plate and that the load is zero at sufficient distance from the origin.

With careful attention to the boundary condition at infinity, our PDE in its time-discretized form, namely equation (21), can be well-approximated by its discrete Fourier transform (DFT) version.³ A very reasonable way to incorporate the DFT is to *assume periodicity* in the spatial variables.⁴ For convenience we will also assume a *square* region. In fact, we assume L is the half-length of a computational domain $(x, y) \in \Omega = [-L, L] \times [-L, L]$. This domain may be substantially larger in practice than the desired region of physical interest $[-L_x, L_x] \times [-L_y, L_y]$. We will apply periodic boundary conditions at $x, y = \pm L$ and we want L to act like ∞ when we do this. See figure 3.

³The *discrete Fourier transform* is the name of the mathematical operation; the FFT is an algorithm for computing the DFT (Briggs & Henson 1995).

⁴Other boundary conditions could be applied along the boundary of Ω —e.g. a clamped condition—but none of the easily implementable choices are obviously superior.

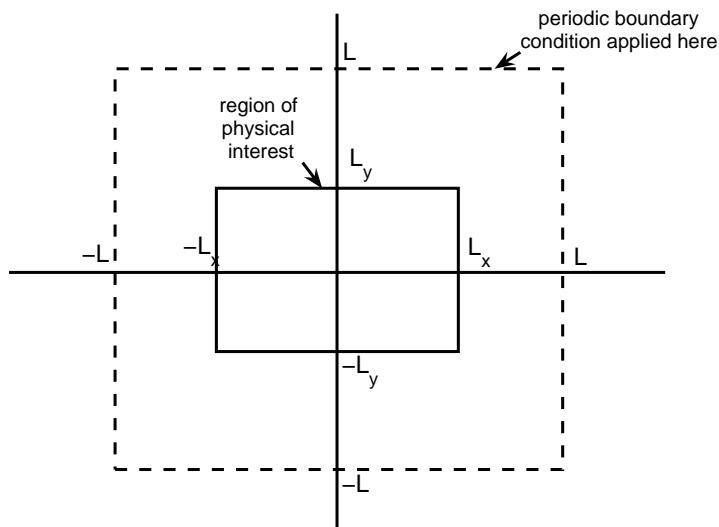


FIGURE 3. Fast Fourier Transform methods require periodicity. We impose periodic boundary conditions significantly far outside the region of modelled load changes or significant deformation.

The PDE problem to which we apply the DFT is, therefore, Equation (21) on the interior of $\Omega = [-L, L] \times [-L, L]$ with periodic boundary conditions on the boundary of Ω , and with the initial condition that $U^0(x, y)$ is known on Ω .

Note that from (21), if $L = \infty$ then the (non-discrete) Fourier transform $\tilde{U}^n = \mathcal{F}_2 U^n$ satisfies iteration

$$\tilde{U}^{n+1}(\xi, \zeta) = \frac{[2\eta\kappa - (\Delta t/2)(\rho_r g + D\kappa^4)] \tilde{U}^n(\xi, \zeta) + \Delta t \tilde{\sigma}_{zz}(\xi, \zeta, t^*)}{2\eta\kappa + (\Delta t/2)(\rho_r g + D\kappa^4)} \quad (22)$$

where $\kappa^2 = \xi^2 + \zeta^2$. This is an easily-computed iteration if one can do the (non-discrete) Fourier transform \mathcal{F}_2 exactly.

To use the DFT we transform the problem to a standard region $\bar{\Omega} = [-\pi, \pi] \times [-\pi, \pi]$. Let $X = \pi x/L$, $Y = \pi y/L$. Then (21) is equivalent to

$$\begin{aligned} & \left(2\eta\mu \bar{\Delta}^{1/2} U^{n+1}\right) + \frac{\Delta t}{2}(\rho_r g U^{n+1} + D\mu^4 \bar{\Delta}^2 U^{n+1}) \\ &= \left(2\eta\mu \bar{\Delta}^{1/2} U^n\right) - \frac{\Delta t}{2}(\rho_r g U^n + D\mu^4 \bar{\Delta}^2 U^n) + \Delta t \sigma_{zz}(X, Y, t^*) \end{aligned} \quad (23)$$

on $\bar{\Omega}$, where $U^n = U^n(X, Y)$, $\mu = \pi/L$, and $\bar{\Delta} = -(\partial^2/\partial X^2 + \partial^2/\partial Y^2)$.

Let N be an integer; typically N is a power of 2 for efficiency in the FFT. Let $h = 2\pi/N$ and let $X_j = -\pi + jh$, $Y_k = -\pi + kh$, $j, k = 1, \dots, N$. On $\bar{\Omega}$ we use the DFT, as normalized by Trefethen (2000), in variables X, Y . If $f(X, Y)$ is some function on $\bar{\Omega}$ with grid values $f_{jk} = f(X_j, Y_k)$ then the DFT (forward, inverse) pair is

$$\hat{f}_{pq} = h^2 \sum_{j,k=1}^N e^{-i(pX_j + qY_k)} f_{jk}, \quad f_{jk} = \frac{1}{(2\pi)^2} \sum_{p,q=-N/2+1}^{N/2} e^{i(pX_j + qY_k)} \hat{f}_{pq}. \quad (24)$$

Let

$$\bar{f}(X, Y) = \frac{1}{(2\pi)^2} \sum_{p, q = -N/2+1}^{N/2} e^{i(pX+qY)} \hat{f}_{pq} \quad (25)$$

be the “band-limited trigonometric interpolant” of $f(X, Y)$ (Trefethen 2000); note the relation to the inverse DFT (24). We see that

$$\bar{\Delta} \bar{f}(X, Y) = \frac{1}{(2\pi)^2} \sum_{p, q = -N/2+1}^{N/2} (p^2 + q^2) e^{i(pX+qY)} \hat{f}_{pq}.$$

That is, the Laplacian $\bar{\Delta}$ on $\bar{\Omega}$ corresponds to multiplying the p, q mode by $(p^2 + q^2)$. Thereby $\bar{\Delta}^{1/2}$ and $\bar{\Delta}^2$ are also defined, respectively, by multiplication by $(p^2 + q^2)^{1/2}$ and $(p^2 + q^2)^2$.

It now follows that (23) is very easy to compute if we approximate $U^n(X, Y)$ by its band-limited interpolant $\bar{U}^n(X, Y)$ and compute the action of the powers of the Laplacian by the multipliers above. This describes a *Fourier spectral collocation method*. That is, one time-step in solving PDE (17) by our method is the sequence

- (i) compute the DFT \hat{U}_{pq}^n by FFT from values $U_{jk}^n \approx U^n(X_j, Y_k) = U^n(x_j, y_k)$; also compute the DFT of the load $(\hat{\sigma}_{zz})_{pq}$ at $t = t^*$ from values $\sigma_{zz}(x_j, y_k, t^*)$,
- (ii) compute

$$\hat{U}_{pq}^{n+1} = \frac{[2\eta\mu(p^2 + q^2)^{1/2} - (\Delta t/2)(\rho_r g + D\mu^4(p^2 + q^2)^2)] \hat{U}_{pq}^n + \Delta t (\hat{\sigma}_{zz})_{pq}}{2\eta\mu(p^2 + q^2)^{1/2} + (\Delta t/2)(\rho_r g + D\mu^4(p^2 + q^2)^2)}, \quad (26)$$

where $\mu = \pi/L$ and

- (iii) undo the DFT (i.e. do the inverse FFT and make sure the result is real) to get $U_{jk}^{n+1} \approx U^{n+1}(X_j, Y_k) = U^{n+1}(x_j, y_k)$.

Compare equation (26) to equation (22) which applies for the non-discrete Fourier transform \tilde{U}^n .

Full MATLAB implementations of the methods in this report are given in Appendix D. Only a few lines of MATLAB are needed to implement the core sequence above, however:

```

for n=0:M-1
    [computations using current displacement uun = U^n(x_j, y_k)]
    uun=uun1;
    [get H = H(x_j, y_k, t^*)]
    sszz=-rhoi*g*H;
    frhs=right.*fft2(uun) + fft2(dt*sszz);
    uun1=real(ifft2( frhs./left ));
end

```

Here “right” and “left” are pre-computed grid values of the expressions $2\eta\mu k - (\Delta t/2)B$ and $2\eta\mu k + (\Delta t/2)B$ which appear in (26), respectively, where $k^2 = p^2 + q^2$ and $B = \rho_r g + D\mu^4 k^4$.

We call the iteration (i), (ii), (iii) the “PDE method” in contrast to the load response matrix method (“LRM method”) of the previous section. With standard estimates on the speed of the FFT when N_x, N_y are powers of two (Briggs & Henson 1995), the “PDE method” requires

$$O(N_x N_y (\log_2 N_x) (\log_2 N_y)) \quad (27)$$

scalar operations to update the vertical displacement. This compares directly to equations (14) and (15) for the “LRM method.” In particular, relative to the $O(N_t N_x N_y (\log_2 N_x) (\log_2 N_y))$ estimate (15) for the “LRM method” using the FFT for convolution we note a factor of N_t less work. Furthermore, the “PDE method” avoids the entire stage of computing the LRM integrals, which turn out to be quite expensive, though totally uninteresting, computations.

Relative to the “LRM method” *without* the FFT, using representative values of $N_t = 25$ and $N_x = N_y = 80$, and assuming that the constants in the “big O notation” are about the same, we get a speed up of about

$$(25 \cdot 80^2 \cdot 80^2) / (80^2 (\log_2 80)^2) \approx 4 \times 10^3.$$

This ratio is roughly what we observe in practice. For instance, on the same computer we compared Fortran 77 codes running the “LRM method” sans FFT using $N_t = 101$ and $N_x = N_y = 31$ with MATLAB codes (Appendix D) implementing the “PDE method” using $N_x = N_y = 32$. We used $\Delta t = 500$ years and bed deformations were computed for 50k years in both cases. The former method took about 10 *hours* while the later took about 4 *seconds* for an observed speedup of about 9×10^3 .

4. DISCUSSION

In the next section we describe the results of computations with the “PDE method.” It is appropriate, however, to first directly address the apparently new feature in PDE (17),

$$\frac{\partial}{\partial t} \left(2\eta \Delta^{1/2} u \right) + \rho_r g u + D \Delta^2 u = \sigma_{zz},$$

namely the viscosity expression “ $\partial/\partial t (2\eta \Delta^{1/2} u)$.”

Within the ice sheet modeling community there is a simplified existing *standard model* for a flat “elastic plate (lithosphere) that overlies a viscous asthenosphere” (Greve 2001, Hagdorn 2003, Zweck & Huybrechts 2005). Comparison to this model illuminates the significance of the viscosity expression in (17). The standard model consists of two equations

$$\rho_r g w + D \Delta^2 w = \sigma_{zz}, \quad (28)$$

$$\frac{\partial u^s}{\partial t} = - \frac{u^s - u_0 - w}{\tau}, \quad (29)$$

where $u^s(x, y, t)$ is the vertical displacement of the earth’s surface, $u_0(x, y)$ is a hypothesized unloaded displacement state, and $w(x, y, t)$ is the position of a notional elastic plate which is in equilibrium with the current load $\sigma_{zz}(x, y, t)$. The essential viscous constant for the standard model is a characteristic time scale τ of relaxation, chosen, for example, as 3000 years by Greve (2001) and Zweck & Huybrechts (2005). The relaxation time τ is indirectly related to the asthenosphere viscosity η ; more on this below.

We can now calculate an illuminating comparison by hand. Suppose that at time $t = 0$ all load is removed but that the vertical displacement is a y -independent sinusoidal mode with spatial frequency k :

$$u(x, y, t=0) = u^s(x, y, t=0) = A_0 \exp(ik\pi x/L). \quad (30)$$

Here A_0 is the initial amplitude and L is a characteristic length scale. We ask: how does such a mode decay in the two models?

Note that the q th power of the Laplacian act on this mode as follows:

$$\Delta^q \exp(ik\pi x/L) = (k^2 \pi^2 / L^2)^q \exp(ik\pi x/L).$$

Thus model (17) has solution $u(x, y, t) = A(t) \exp(ik\pi x/L)$ where

$$2\eta(|k|\pi/L)\dot{A} + \rho_r g A + D(k^4 \pi^4 / L^4)A = 0.$$

That is, in model (17) the amplitude of the k mode satisfies

$$\dot{A} = -\frac{\rho_r g L^4 + D k^4 \pi^4}{2\eta L^3 |k| \pi} A, \quad A(t=0) = A_0, \quad (31)$$

so a mode with frequency k decays a rate that depends upon k . By contrast, in model (28), (29) with $u_0 = 0$ the same mode evolves by

$$\dot{A} = -\frac{1}{\tau} A, \quad A(t=0) = A_0 \quad (32)$$

because $w = 0$ as the load has been removed; equation (29) reduces to $\partial u^s / \partial t = -\tau^{-1} u^s$. Here we see that all modes decay at a rate independent of the frequency.

But it is clearly the case that a viscous asthenosphere will make elastic plate modes decay at different rates depending on the frequency. Indeed, Greve (1997) identifies the failure of the standard model (28), (29) to have frequency dependent relaxation times as a deficiency of that model relative to full spherical self-gravitating models. Comparing equation (31) to (32) we are motivated to plot the function

$$\tau(k) = \frac{2\eta L^3 |k| \pi}{\rho_r g L^4 + D k^4 \pi^4}, \quad (33)$$

which has units of time. Supposing $L = 2000$ km and that ρ_r, g, D, η have the values given in section 1, we plot $\tau(k)$ in figure 4. We see that the standard choice $\tau = 3000$ a in (32) corresponds to frequencies $k \approx 1$ and $k \approx 10$ in (31), but that no constant relaxation time is representative of the actual relaxation spectrum.

Furthermore we see in formula (33) and figure 4 that for small k (e.g. $k \lesssim 3$) the relaxation time $\tau(k)$ is proportional to k . This behavior is identified by (Klemann & Wolf 1999)—see Greve (2001, section 5)—as correct for the most significant mode in a spherical, self-gravitating viscoelastic earth model.

The justification for model (28), (29) is its computability, of course. Indeed, the computation of the elliptic PDE (28) is standard in all numerical paradigms (finite difference, finite element, spectral). At least on a rectangular spatial grid, however, the time-semidiscretization (21) of equation (17) is just as computable as (28). In particular, if an ice sheet simulation is performed on a rectangular grid using a finite difference or finite element method for the ice dynamics then equation (17) can be easily computed by the Fourier spectral collocation method of the previous section.

Now we come to another reason to prefer equation (17) as a model for earth deformation in the context of ice sheet modeling. Let us suppose that at the current time the ice thickness H_0 (and possibly water depth, giving an effective ice thickness) in a region of interest has been well-measured. Let us suppose that a reasonably detailed map of current uplift rate $\dot{u}_0 = \partial u / \partial t$ is also known. This is a realistic supposition given the state of observational geophysics circa 2006 because uplift can be well-constrained by GPS measurements (Larsen and others 2005) when bedrock is exposed. Alternatively a spherical viscoelastic earth model

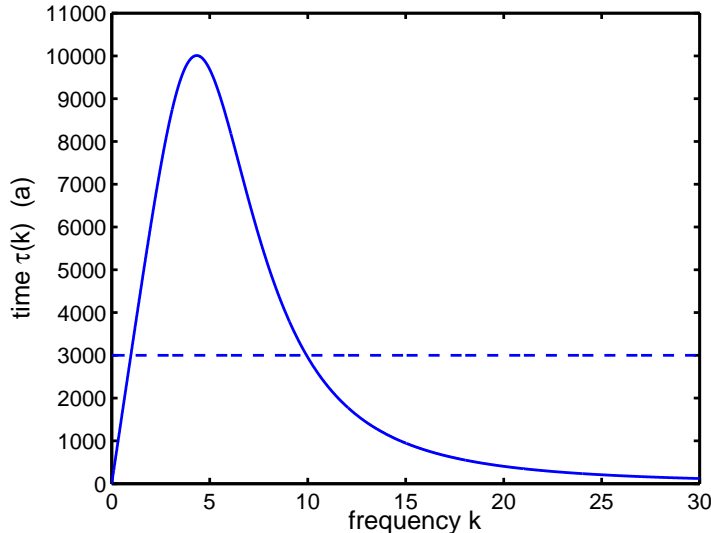


FIGURE 4. Frequency dependent relaxation time $\tau(k)$ (solid) for mode k in equation (30). The value $\tau = 3000$ a (dashed) for the standard model is a reasonable constant value, but no constant provides a good fit.

of more-or-less arbitrary sophistication and computational expense might generate a trusted current uplift map (Ivins & James 2005). In either case we can then use (17) to determine the initial condition for the earth deformation part of an ice sheet simulation without requiring further reference to an assumed past load history; compare the integration over load history scheme used in (Lingle & Clark 1985). In fact, by (17) we may solve

$$\rho_r g u_0 + D \Delta^2 u_0 = \rho_i g H_0 - 2\eta \Delta^{1/2} \dot{u}_0 \quad (34)$$

for u_0 to get the starting displacement. In other words we ask for the “pre-bent” position of the elastic plate in the half space model which accounts for the current uplift rate using the current load (i.e. current effective ice thickness). Solving (34) numerically is no harder than, in fact it amounts to, one step of the numerical method already described. If the load does not change in the simulation, an uninteresting case for ice sheets of course, then the elastic plate overlying the viscous half space will start at the current time with the current uplift but will then relax to the state satisfying equation (18) for equilibrium with the load and buoyant force, and there will no more uplift. Note that the presence of bed topography is completely irrelevant here because of the linear nature of the model; see comments in (Lingle & Clark 1985) to the effect that bed topography represents a irregular “thin veneer of zero strength” atop an elastic plate lithosphere of (significant) flexural rigidity D .

The mechanism described in the previous paragraph is, we believe, a more principled replacement for the hypothesized “unloaded surface elevation” $u_0(x, y)$ used in the standard model (28), (29). Use of that standard model seems to require an assumption of present day isostatic equilibrium with the current load (Zweck & Huybrechts 2005) or other artificial assumption which is in conflict with observed spatially-varying current uplift.

An entirely different class of viscoelastic earth models exists in the literature, of course. These are the layered, spherical, self-graviating viscoelastic models which typically descend

from the work of Cathles (1975) and/or Peltier (1974). The numerical implementation of these models typically involves computing a high degree spherical harmonic expansion of the strain field for the entire three-dimensional geoid. The traditional difficulty with these models is their computational cost (Fastook 1999, Greve 2001). Furthermore there is only modest benefit because results from the standard model (28), (29) above, in particular, are regarded by the ice sheet modeling community as reasonably close to those from the spherical models (Greve 2001). Equation (17) is promising because it is just as computationally inexpensive as the standard model but incorporates at least one important feature of the spherical models, namely frequency dependent relaxation times.

Speaking mathematically, an interesting additional possibility exists within the same class of computationally inexpensive ‘‘PDE methods.’’ Namely, one should be able to modify equation (17) to take spherical effects into account. In particular, equation (17) would be computable at essentially the same speed if it were replaced by a non-constant coefficient version, for instance

$$\frac{\partial}{\partial t} \left(2\eta(x, y)\Delta^{1/2}u \right) + \rho_r g \alpha(x, y)u + D(x, y)\Delta(\beta(x, y)\Delta u) = \sigma_{zz}. \quad (35)$$

We do not currently know that a set of non-constant coefficients η, D, α, β exist which correctly account for spherical geometry. It seems, however, that classical continuum mechanics and differential geometry must produce such a form because the standard model for a spherical self-gravitating earth is a *linear* model. That is, it has linear response to load. Abstractly, this linearity is all that is necessary to make it inevitable⁵ that a two (spatial) dimension, non-constant coefficient linear equation for the vertical displacement of the earth’s surface must exist for each patch of the earth’s surface. It may well involve additional pseudo-differential operators not present in the putative form (35), however.

5. NUMERICAL RESULTS

A ‘‘tweak’’ to the procedure. It turns out that a small error can be avoided if the ‘‘PDE method’’ is modified slightly. In fact, in verifying the ‘‘PDE method’’ below, using an exact integral formula for a disc load, we observed that there was a uniform error of several meters. This uniform error decayed slowly as the distance at which the periodic boundary condition was applied went to infinity.

The following simple modification eliminates this error. Using the notation of section 3, consider $U^n(x_j, y_k)$ on the grid at timestep n . Let \bar{U}_L^n be the average value of U^n along the boundary of the computational domain $\Omega = [-L, L] \times [-L, L]$; recall Ω is typically larger than the physical region $[-L_x, L_x] \times [-L_y, L_y]$. Let $u_{H_0, R_0}^\infty(r)$ be the vertical displacement at distance r from the center of an ice disc load of thickness H_0 and radius R_0 of an elastic plate in equilibrium with the buoyant restoring force. That is, let $u_{H_0, R_0}^\infty(r)$ be the value from formula (44) in Appendix B. Choose the values H_0, R_0 so that the volume $\pi R_0^2 H_0$ of the disc load matches the current (timestep n) load volume, or rather its ice equivalent volume if appropriate.

Our ‘‘tweak’’ replaces the solution $U^n(x_j, y_k)$ at each timestep n with values to which a constant shift has been applied:

$$U^{n,\circ}(x_j, y_k) = U^n(x_j, y_k) - \bar{U}_L^n + u_{H_0, R_0}^\infty(L). \quad (36)$$

⁵See the discussion of distributions in (Reed & Simon 1980), for instance.

That is, we want the “far-field value” produced by the original “PDE method” to be thrown out and replaced by the equilibrium plate value with an equivalent disc load. Though the volume of the equivalent disc is determined by the current load, one obviously has some freedom in choosing its thickness and radius. We presume that an effort is made to approximate the aspect ratio of the actual load, but close matching is not essential. In fact the Green’s function value would work reasonably well, too.

Verification. The first concern regarding computations with our earth deformation model is *verification*. In particular, we want to know if numerical results from the “PDE method”, with the just-mentioned “tweak,” are close to highly-accurate solutions of the continuum equation (17). In seeking such solutions we inevitably come to disc loads. Appendix B addresses this case by the Hankel transform. It yields equation (43), an integral formula for the time-dependent radially-symmetric deflection $u^V(r, t)$ resulting from the application (at time zero) of a disc load; see figure 16. The integral must be computed numerically, but numerical quadrature is an approximation completely independent of the cartesian-grid- and FFT-based “PDE method.” We use integral formula (43) as an “exact” solution, believing the accuracy of our numerical integration of (43) to exceed that of the “PDE method” for any achievable grid.

Our MATLAB implementation of the “PDE method” is the function `fastearth.m` listed in Appendix D. Also listed are implementations of the LRM method for the spherical elastic earth model (`geforconv.m`) and the numerical integration of equation (43) (`viscdisc.m`).

Let us define a particular numerical experiment. Suppose we use the parameters specified in section 1: $D = 5.0 \times 10^{24}$ N m, $\rho_r = 3300$ kg m $^{-3}$, and $\eta = 10^{21}$ Pa s. Suppose the disc of ice (density $\rho_i = 910$ kg m $^{-3}$) has radius 1000 km and thickness 1000 m. We seek the deflection on a square region R , centered on the disc load, of side length 4000 km ($L_x = L_y = 2000$ km). Suppose that at time zero the deflection is identically zero, and suppose that the load is applied at that time. We calculate the deflection at $t = 20k$ years as computed by the “PDE method” and by formula (43).

There are *three* numerical parameters of importance for the “PDE method”:

- N , the number of grid points in each direction,
- Z , the factor by which the computational domain $\Omega = [-L, L] \times [-L, L]$ is larger than the physical domain $[-L_x, L_x] \times [-L_y, L_y]$; here $L_x = L_y$, and
- Δt , the time step used in approximating the time derivative which occurs in equation (17).

Our verification involves showing that as these parameters go to their continuum limits ($N \rightarrow \infty$, $Z \rightarrow \infty$, $\Delta t \rightarrow 0$) we approach the “exact” solution (43).

For verification we first fixed $\Delta t = 100$ years and considered the effect of grid refinement and of changes to the distance at which the periodic boundary condition was applied. Regarding grid refinement we considered N ranging over powers of two from $2^3 = 8$ to $2^8 = 256$. Regarding the distance to the periodic boundary condition we imposed the periodic boundary condition at $|x|, |y| = L$, where $L = Z L_x = Z L_y$, and we used $Z = 1, 2, 4, 8$, but we quickly discovered that with the above-mentioned “tweak” any value $Z \geq 2$ works fine; not shown.

The result for *maximum error* under grid refinement is shown in figure 5. This maximum error is not the only reasonable measure. As shown in figure 6, for fine grids errors greater

than one meter are highly localized to certain points just at the edge of the disc load. Note realistic ice loads do not have margins as sharp as this disc load. For these reasons among others it is reasonable to consider average errors, and we see in figure 7 that the average errors are less than 20 cm for $N = 256$, or roughly 0.07% of the compensation depth.

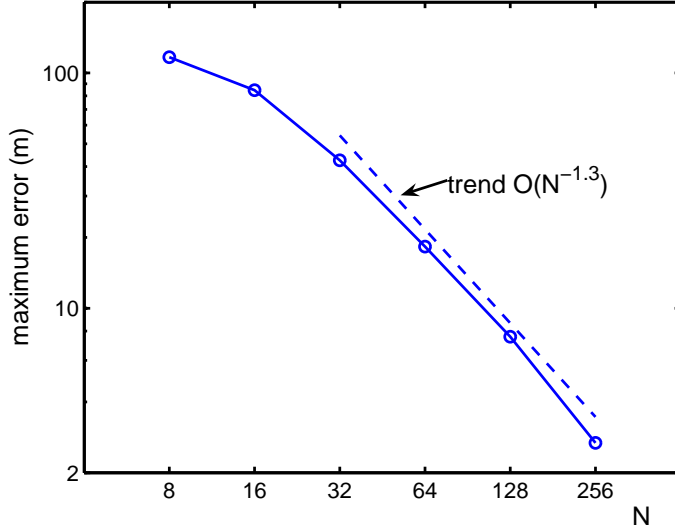


FIGURE 5. Maximum error made by the “PDE method” relative to the Hankel transform integral (43). Grid refinement (increasing N) reduces the max error to below 3 m when $N = 256$. Here $Z = 2$ and $\Delta t = 100$ a.

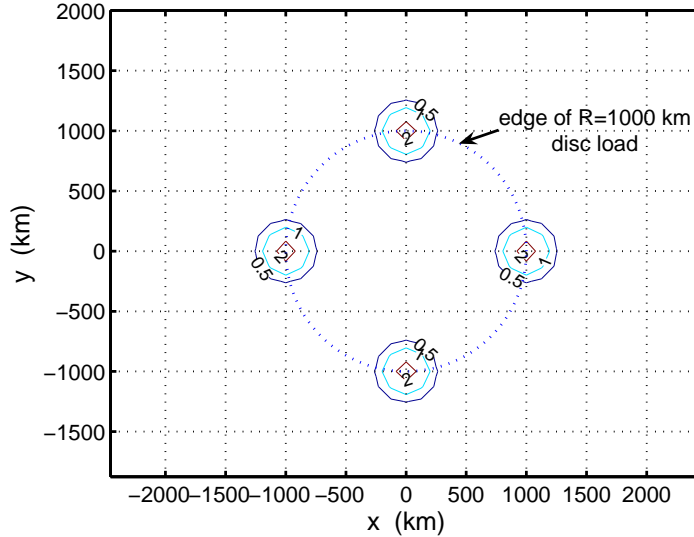


FIGURE 6. Spatial distribution of the error when $N = 256$, $Z = 2$, and $\Delta t = 100$ a. Contours of the error $|(PDE \text{ method}) - (\text{equation (43)})|$ at 0.5, 1, 2 m. The error is concentrated where the edge of the disc load meets the coordinate axes.

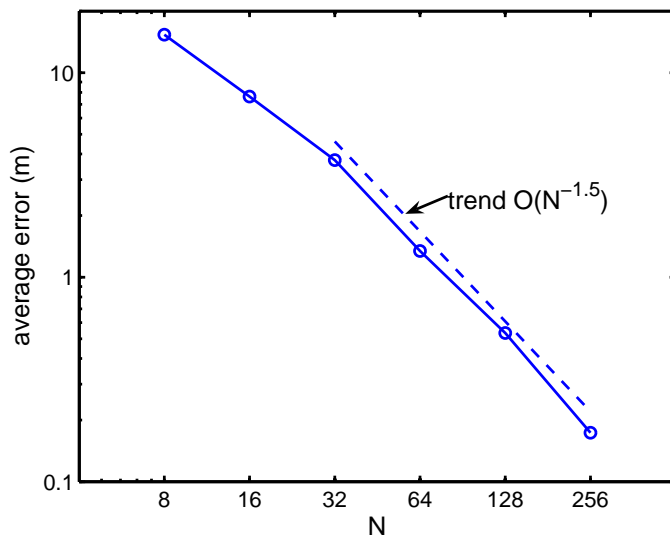


FIGURE 7. Same as figure 5 but now *average* error. Grid refinement (increasing N) reduces the average error to below 20 cm when $N = 256$.

Next we compare the effects of spatial grid refinement, increasing N , to reduction of time stepsize Δt on the error. See figure 8. We see that any value of Δt less than 500 years is fine; this is great news for ice sheet simulation. It is not, however, surprising because of the relative timescales of ice versus asthenosphere flow.

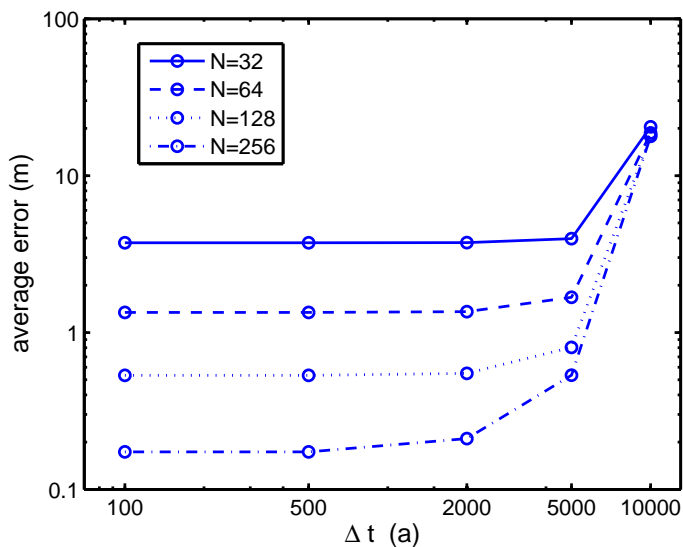


FIGURE 8. Average error as in figure 7 but with Δt varying, and for several values of N . There is no need for $\Delta t < 500$ a. Spatial grid refinement (increasing N) is more important to reducing error than is temporal refinement (decreasing Δt).

Ice sheet modeling. Earth deformation used in the context of ice sheet modeling is our actual interest. Earth deformation is obviously effected by ice sheet flow—the load moves around. Conversely, as the bed deforms the surface slope of the ice sheet changes and this effects flow. There is non-trivial coupling.

The reasonable simplest ice sheet model is the isothermal model with Glen rheology (Paterson 1994, Nye 2000). Let $h(x, y, t)$ be the surface elevation of the ice and let $H(x, y, t)$ be the ice thickness. The frozen-base isothermal ice sheet equation is the single nonlinear diffusive partial differential equation

$$\frac{\partial H}{\partial t} = M + \nabla \cdot (\Gamma H^{n+2} |\nabla h|^{n-1} \nabla h) \quad (37)$$

where n is the Glen exponent, e.g. $n = 3$, and Γ is a constant (typically $\Gamma = 2(\rho_i g)^n A_0 / (n+2)$ where A_0 is a softness parameter). If $b(x, y, t)$ is the ice sheet bed elevation—a slight change of notation from the rest of the paper—then of course $h = b + H$.

As we now show, exact similarity solutions to this equation which incorporate simple isostasy (Nye 2000, Bueler et al. 2005; compare Halfar 1983) provide a very nice tool to examine coupling to the earth model. They help illuminate the differences among earth models. By “simple isostasy” we mean the rule which specifies

$$b = -fH \quad (38)$$

where f is a fixed fraction of the ice thickness (Nye 2000); we will let $f = \rho_i / \rho_r = 0.27576$ in our numerical experiments. Since $h = b + H$, if equation (38) applies then $h = (1 - f)H$.

We will compare numerical results for three coupled ice sheet flow/earth deformation models:

SIMPLE:	equations (37) and (38),
STANDARD:	equations (37), (28), (29), and $b = u^s$,
LINGLE&CLARK:	equations (37), (1), (17), and $b = u^E + u^V$.

Figure 9 shows a result of a coupled simulation for these three models. A detail near the margin is shown in figure 10.

In fact, the result shown in figure 9 came from starting with $H = 0$ and $b = 0$ at $t = 0$ and using an accumulation history corresponding to the similarity solution illustrated by figure 11. That is, the accumulation $M(x, y, t)$ comes from equations (9) and (10) in (Bueler et al. 2005), using $f = 910/3300$, $\lambda = 5$, $\alpha = -1$, $\beta = 2$, $H_0 = 3600$ m, $R_0 = 750$ km, $\Gamma = 9.0177 \times 10^{-13}$ m⁻³ s⁻¹, and with the additional statement $M = 5t^{-1}H_\lambda$. Note $t_0 = 40034$ years. In addition, at time $t = t_0$ the accumulation is turned off and so for $t > t_0$ the exact behavior of the solution to SIMPLE is a Halfar-type (Halfar 1983) accumulation-free solution. Thus the accumulation history is from a similarity solution to equation (37), incorporating simple isostasy, which grows from zero at $t = 0$ to maximum height at $t_0 = 40034$ years and spreads out from then on, with no loss of volume.

The importance of such a similarity solution is that it forms an *exact* continuum solution to the SIMPLE model. Therefore we can answer with some precision the question “*how do differences resulting from coupling to various earth deformation models compare to the numerical errors which occur in ice sheet modeling?*” This is an important question. If numerical ice sheet errors demonstrably exceed the earth model differences then we should be skeptical of any expenditure of effort in the earth modeling direction. Conversely, even

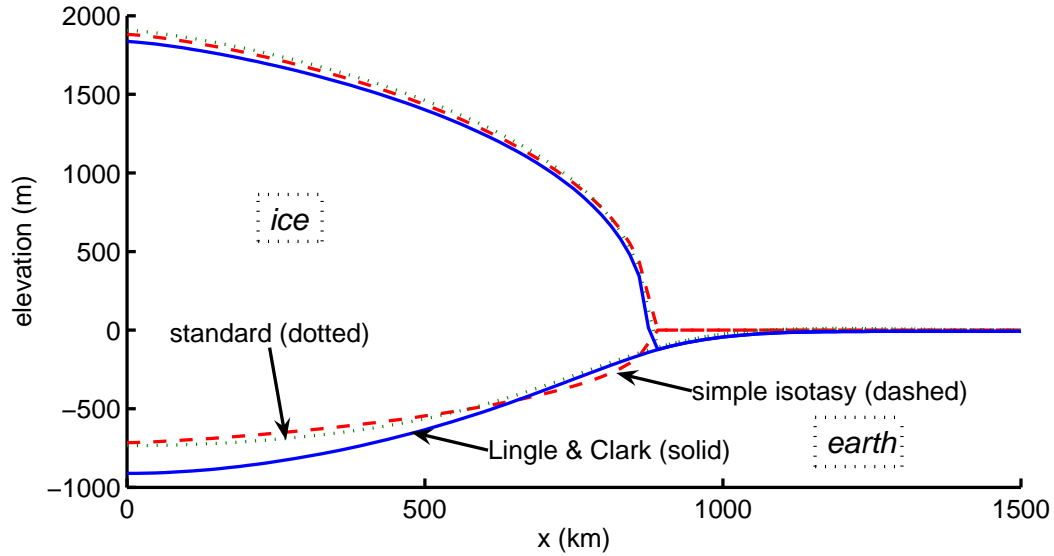


FIGURE 9. Ice sheet on deforming bed, at time 60k years, from three earth models SIMPLE, STANDARD, and LINGLE&CLARK. View of gridded numerical values ($N_x = N_y = 192$) along the positive x -axis of the grid.

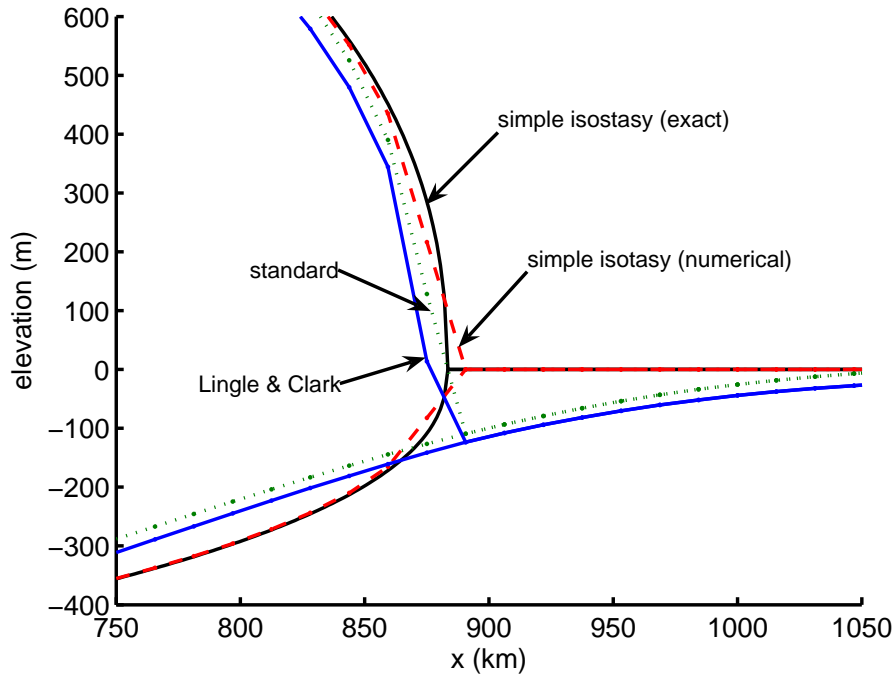


FIGURE 10. See figure 9; detail near the grounded margin. Exact similarity solution to the simple isostasy model is added (solid).

if the differences among earth models are significant, one should report these differences relative to the actual magnitude of numerical ice modeling errors.

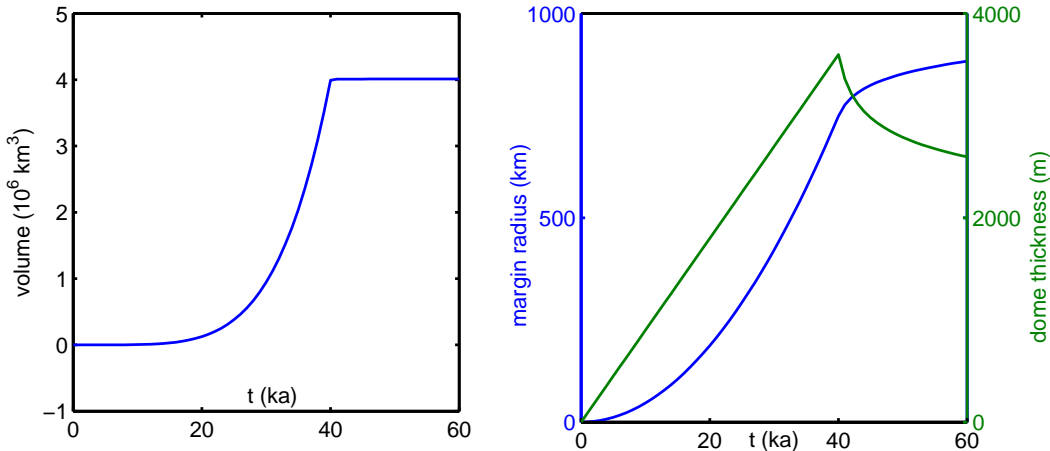


FIGURE 11. Views of a similarity solution to equation (37). Left: volume over time. Right: margin radius (solid) and dome height (dashed) over time. At time $t_0 = 40034$ a the solution switches from growing ($\lambda = 5$) to Halfar ($\lambda = 0$), in both cases with simple isostasy ($f = 910/3300$).

Figure 9 indeed suggests differences among the coupled models. We ran each model to final time $t = 60k$ a. As shown in figure 12, however, all of the models produce the same volume at the final time, and indeed at all times; this follows from using the same finite difference approach for the ice flow (as described in (Bueler et al. 2005)) and, of course, the same accumulation history $M(x, y, t)$. So the differences can be described by the distributions of ice thickness. In figure 13 we show the maximum and average of the pairwise absolute thickness differences $|H_{\text{SIMPLE}} - H_{\text{STANDARD}}|$, etc. (The average differences are over the $H > 0$ grid points under SIMPLE.) We see average thickness differences greater than 10 m between each pair. We see that the greatest pairwise difference is between SIMPLE and LINGLE&CLARK; compare figure 9.

We see a similar picture for bed elevation differences, with SIMPLE versus STANDARD showing somewhat smaller differences, and the comparison SIMPLE versus LINGLE&CLARK again being largest.

Now, are these differences significant? The answer shown in figure 15 is *yes*. With a caveat. As noted in (Bueler et al. 2005), ice sheet flow simulations on grids inevitably make large thickness errors near the margin. These errors decay only slowly under grid refinement, as can be seen in figure 15.

6. CONCLUSIONS

We have seen several modeling and computational issues and numerous equations. So let us identify our major point: Equation (17)

$$\frac{\partial}{\partial t} \left(2\eta \Delta^{1/2} u \right) + \rho_r g u + D \Delta^2 u = \sigma_{zz},$$

where Δ is the positive Laplacian $\Delta = -\partial^2/\partial x^2 - \partial^2/\partial y^2$, is *both*

- a better model for a viscous half space overlain by an elastic plate than the standard model (28), (29) which is widely used in the ice sheet modeling literature,

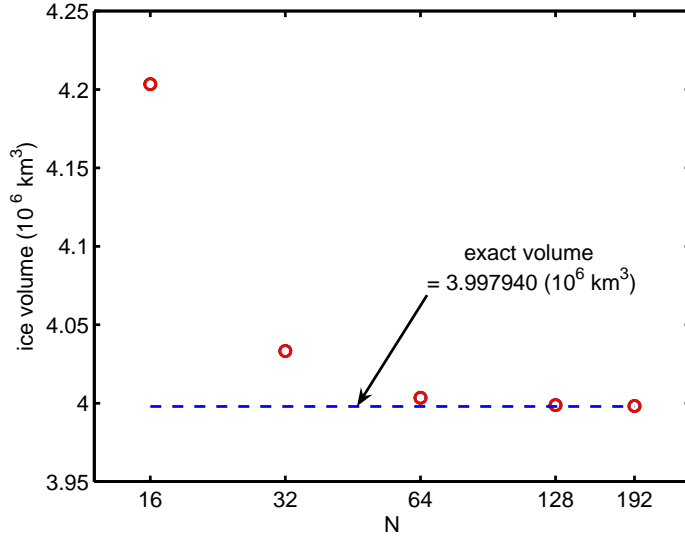


FIGURE 12. All models have identical convergence of numerical volume at $t = 60k$ a; they share the same accumulation history.

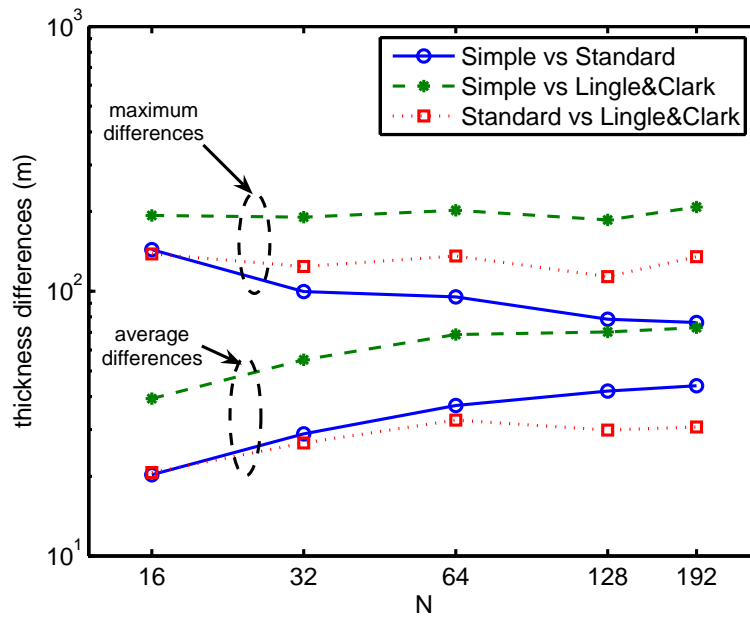


FIGURE 13. Maximum and average *ice thickness* differences in pairwise comparison.

- *and* is very computationally tractable on a rectangular grid using a Fourier spectral collocation method.

In brief, one derives equation (17) by starting with equation (4) in (Lingle & Clark 1985), clearing denominators, and then taking the inverse Hankel transform by recognizing powers of the positive Laplacian Δ . That is, equation (17) is equivalent to equation (4) in (Lingle & Clark 1985).

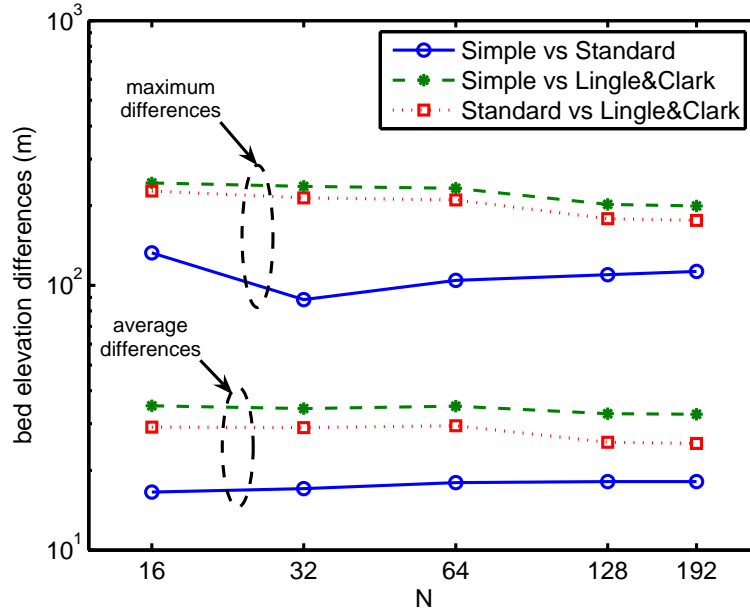


FIGURE 14. Maximum and average *bed elevation* differences in pairwise comparison.

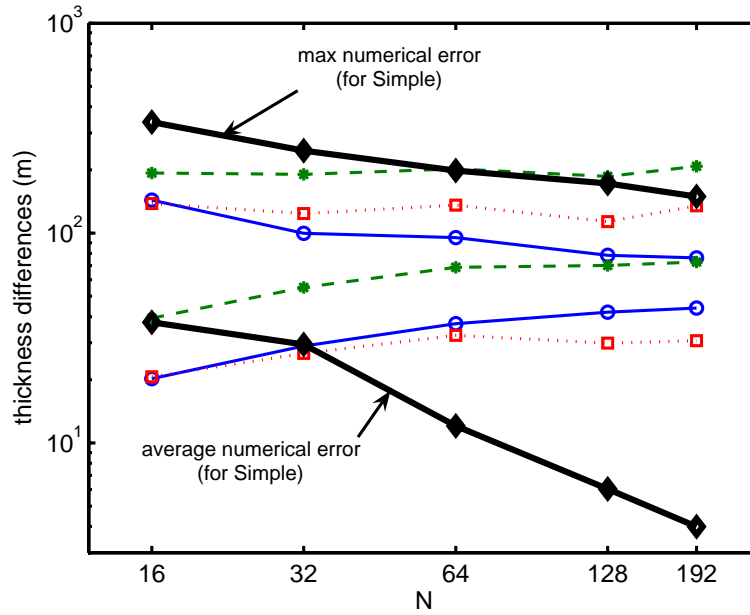


FIGURE 15. Ice thickness differences in pairwise comparison as in figure 13 but with numerical errors for the simple isostasy case superimposed. Differences among coupled ice-earth models significantly exceed numerical error except for localized numerical errors within a couple of grid points of the margin.

Of course, equation (17) fails to incorporate spherical or self-gravitating effects. Following Lingle & Clark (1985) we have, however, chosen to superpose upon the result of (17) a purely-elastic, but spherical and self-gravitating (Farrell 1972), displacement from equation (1). This is an admittedly *ad hoc* way to incorporate spherical and self-gravitating effects into an earth deformation model.⁶ We note that the effects of equation (1) are “longer range” than those of equation (17) at large times, so in some sense it is more important to incorporate “sphericalness” into the purely elastic part of the earth model.

7. ACKNOWLEDGEMENTS AND A DEDICATION

Praveena Muthyala and Chris Larsen contributed to its practical and conceptual development, respectively. It is dedicated to the students in Math 611 in Fall 2005, who suffered from the first author’s need to be thorough on the subject of Hankel transforms.

REFERENCES

- Bracewell, R. N. (1978), *The Fourier Transform and Its Applications*, 2nd edn, McGraw-Hill Book Company, New York.
- Briggs, W. L. & Henson, V. E. (1995), *The DFT: An Owner’s Manual for the Discrete Fourier Transform*, SIAM Press, Philadelphia.
- Bueler, E., Lingle, C. S., Kallen-Brown, J. A., Covey, D. N. & Bowman, L. N. (2005), ‘Exact solutions and numerical verification for isothermal ice sheets’, *J. Glaciol.* **51**(173), 291–306.
- Cathles, L. M. (1975), *The Viscosity of the Earth’s Mantle*, Princeton University Press, Princeton, NJ.
- Farrell, W. E. (1972), ‘Deformation of the earth by surface loads’, *Rev. Geophysics and Space Physics* **10**(3), 761–797.
- Fastook, J. L. (1999), A computationally efficient bedrock isostasy model. unpublished.
- Greve, R. (1997), ‘A continuum–mechanical formulation for shallow polythermal ice sheets’, *Phil. Trans. Royal Soc. London A* **355**, 921–974.
- Greve, R. (2001), Glacial isostasy: Models for the response of the Earth to varying ice loads, *in* B. Straughan et al., eds, ‘Continuum Mechanics and Applications in Geophysics and the Environment’, Springer, pp. 307–325.
- Hagdorn, M. K. M. (2003), Reconstruction of the past and forecast of the future European and British ice sheets and associated sealevel change, PhD thesis, The University of Edinburgh.
- Halfar, P. (1983), ‘On the dynamics of the ice sheets 2’, *J. Geophys. Res.* **88**(C10), 6043–6051.
- Ivins, E. R. & James, T. S. (2005), ‘Antarctic glacial isostatic adjustment: a new assessment’, *Antarctic Science* **17**(4), 537–549.
- Klemann, V. & Wolf, D. (1999), ‘Implications of a ductile crustal layer for the deformation caused by the fennoscandian ice sheet’, *Geophys. J. Int.* **139**, 216–226.
- Larsen, C. F., Motyka, R. J., Freymuller, J. T., Echelmeyer, K. A. & Ivins, E. R. (2005), ‘Rapid viscoelastic uplift in southeast Alaska caused by post-Little Ice Age glacial retreat’, *Earth and Planetary Science Letters* **237**, 548–560.
- Lingle, C. S. & Clark, J. A. (1985), ‘A numerical model of interactions between a marine ice sheet and the solid earth: Application to a West Antarctic ice stream’, *J. Geophys. Res.* **90**(C1), 1100–1114.
- Morton, K. W. & Mayers, D. F. (1994), *Numerical Solutions of Partial Differential Equations: An Introduction*, Cambridge University Press.
- Nye, J. F. (2000), ‘A flow model for the polar caps of Mars’, *J. Glaciol.* **46**(154), 438–444.
- Paterson, W. S. B. (1994), *The Physics of Glaciers*, 3rd edn, Pergamon.
- Peltier, W. R. (1974), ‘The impulse response of a Maxwell earth’, *Rev. Geophys. Space Phys.* **12**, 649–669.
- Reed, M. & Simon, B. (1980), *Methods of Modern Mathematical Physics I*, 2nd edn, Academic Press.
- Sneddon, I. N. (1951), *Fourier Transforms*, McGraw-Hill Book Company, New York.

⁶The *ad hoc* combination “ $u = u^E + u^V$ ” could perhaps be replaced by some other linear combination $u = \alpha u^E + \beta u^V$, $\alpha, \beta > 0$, however.

Trefethen, L. N. (2000), *Spectral Methods in MATLAB*, SIAM Press.

van der Veen, C. J. (1999), *Fundamentals of Glacier Dynamics*, Balkema.

Zweck, C. & Huybrechts, P. (2005), ‘Modeling of the northern hemisphere ice sheets during the last glacial cycle and glaciological sensitivity’, *J. Geophysical Research* **110**. D07103, doi:10.1029/2004JD005489.

APPENDIX A. ON THE HANKEL TRANSFORM AND POWERS OF THE LAPLACIAN

A reasonable first reference for the Hankel transform is Chapter 12 of (Bracewell 1978). Sneddon (1951) is much more complete, however. Sneddon addresses the application of Hankel transforms to elasticity problems, in particular.

Definition. Suppose $f(r)$ is defined on $(0, \infty)$ and suppose that $\int_0^\infty |f(r)| r dr < \infty$. The *Hankel transform* $\bar{f}(\kappa)$, $\kappa > 0$, is

$$\bar{f}(\kappa) = \int_0^\infty f(r) J_0(\kappa r) r dr. \quad (39)$$

This is the transform as normalized by (Sneddon 1951), (Cathles 1975), and (Lingle & Clark 1985); Bracewell (1978) is slightly different.

Here J_0 is the zeroth-order Bessel function of first kind

$$J_0(z) = \sum_{k=0}^{\infty} \frac{(-1)^k}{2^{2k} (k!)^2} z^{2k},$$

an entire function; note $|J_0(r)| \leq 1$ for all r . $J_0(z)$ is the unique solution to the ODE initial value problem

$$z^2 y''(z) + zy'(z) + (z^2 - 0)y(z) = 0, \quad y(0) = 1, \quad y'(0) = 0 \quad (40)$$

and it has integral formula

$$J_0(z) = \frac{1}{2\pi} \int_0^{2\pi} e^{-iz \cos \theta} d\theta. \quad (41)$$

Both (40) and (41) will be used below.

The most natural source of the Hankel transform is as the *Fourier transform of a radial function on the plane*. In particular, suppose $f(x, y)$ is a bounded and integrable function on the plane which is actually radial $f = f(r)$. Suppose one computes the two-variable Fourier transform $\mathcal{F}_2[f] = \tilde{f}$ by converting the integral to polar coordinates:

$$\begin{aligned} \tilde{f}(\xi, \zeta) &= \frac{1}{2\pi} \int_{-\infty}^{\infty} \int_{-\infty}^{\infty} f(r) e^{-i(x\xi + y\zeta)} dx dy = \int_0^\infty f(r) \left[\frac{1}{2\pi} \int_0^{2\pi} e^{-ir\kappa \cos(\theta - \phi)} d\theta \right] r dr \\ &= \int_0^\infty f(r) \left[\frac{1}{2\pi} \int_0^{2\pi} e^{-ir\kappa \cos \theta} d\theta \right] r dr = \int_0^\infty f(r) J_0(\kappa r) r dr \end{aligned}$$

where $\kappa^2 = \xi^2 + \zeta^2$. We have used (41) above. Concretely, we have substituted $x = r \cos \theta$, $y = r \sin \theta$, $\xi = \kappa \cos \phi$, and $\zeta = \kappa \sin \phi$. Thus $x\xi + y\zeta = r\kappa \cos(\theta - \phi)$, and for fixed ϕ the function $\varphi(\theta) = e^{-ir\kappa \cos(\theta - \phi)}$ is periodic with period 2π . We conclude that in these circumstances \tilde{f} is also radial.

The Hankel transform (39) is evidently linear. The general two-variable Fourier transform, which we have normalized to be unitary, has the property

$$\tilde{\tilde{g}}(x, y) = g(-x, -y).$$

Therefore the map $g \mapsto \tilde{g}$ is the identity when restricted to the subspace of radial functions, so $\bar{f}(r) = \tilde{f}(r) = f(r)$ and the Hankel transform is self-inverse.

For $f = f(x, y)$ sufficiently smooth, define the *positive Laplacian* of f to be

$$\Delta f = -\nabla^2 f = -\frac{\partial^2 f}{\partial x^2} - \frac{\partial^2 f}{\partial y^2}.$$

We have chosen the sign of the Laplacian to be positive *as an operator*, which is to say that the eigenvalues/spectrum of this operator are nonnegative. In particular, the Fourier transform of the Laplacian is multiplication by a nonnegative function

$$\widetilde{\Delta f}(\xi, \zeta) = (\xi^2 + \zeta^2) \tilde{f}(\xi, \zeta).$$

For a radial function $f(r)$ we recall that $\Delta f(r) = -f'' - r^{-1}f'$.

Consider the Hankel transform of the Laplacian.

Lemma. *If $f'(r)$ is bounded as $r \rightarrow 0^+$ and if $\max\{|f(r)|r, |f'(r)|r\} \rightarrow 0$ as $r \rightarrow +\infty$ then the Hankel transform formula holds:*

$$\overline{\Delta f}(\kappa) = \kappa^2 \bar{f}(\kappa).$$

Proof. Letting prime denote $\partial/\partial r$, two integrations-by-parts do the job:

$$\begin{aligned} & \int_0^\infty (-f''(r) - r^{-1}f'(r))J_0(\kappa r)r \, dr \\ &= f'(r)J_0(\kappa r)r \Big|_0^\infty + \int_0^\infty f'(r)\frac{\partial}{\partial r}(J_0(\kappa r)r) \, dr - \int_0^\infty f'(r)J_0(\kappa r) \, dr \\ &= 0 + \int_0^\infty f'(r)[J_0'(\kappa r)\kappa r] \, dr = f(r)J_0'(\kappa r)\kappa r \Big|_0^\infty - \int_0^\infty f(r)(J_0'(\kappa r)\kappa r)' \, dr \\ &\stackrel{*}{=} 0 - \int_0^\infty \frac{f(r)}{r}(z^2 J_0''(z) + zJ_0'(z)) \, dr \stackrel{\dagger}{=} - \int_0^\infty \frac{f(r)}{r}(-z^2 J_0(z)) \, dr \\ &= \kappa^2 \int_0^\infty f(r)J_0(\kappa r)r \, dr = \kappa^2 \bar{f}(\kappa). \end{aligned}$$

We substituted $z = \kappa r$ in step $*$ to recognize Bessel's equation (40) in step \dagger . \square

It follows that also for powers of the Laplacian we can give nice Hankel transform formulae. In particular, if

$$\Delta^2 = \nabla^4 = \frac{\partial^4}{\partial x^4} + 2\frac{\partial^4}{\partial x^2 \partial y^2} + \frac{\partial^4}{\partial y^4}$$

denotes the biharmonic operator (Sneddon 1951), and if $f(r)$ is radial and has appropriate boundedness, then

$$\overline{\Delta^2 f}(\kappa) = \kappa^4 \bar{f}(\kappa).$$

Now we define the *positive square root* $\Delta^{1/2}$ of the Laplacian Δ via the Fourier transform:⁷

Definition. Define $(\Delta^{1/2}f)(x, y)$ by

$$\widetilde{\Delta^{1/2}f}(\xi, \zeta) = (\xi^2 + \zeta^2)^{1/2} \tilde{f}(\xi, \zeta).$$

⁷The Fourier transform gives a spectral resolution of the positive operator Δ acting on the plane, subject to appropriate boundedness at infinity (Reed & Simon 1980). Thus we are using the functional calculus to define $\Delta^{1/2}$.

Note that $\Delta^{1/2}$ acts on scalar functions to produce scalar functions but that it is not a true differential operator. In particular, it is neither the gradient nor the divergence. It can, however, be easily calculated using the Hankel transform because the following formula applies for radial functions $f = f(r)$:

$$\overline{(\Delta^{1/2} f)}(\kappa) = \kappa \bar{f}(\kappa).$$

Finally we consider the Hankel transform of the Dirac delta “function.” Care must be taken because the delta function we need is a function only of the radial coordinate while its defining property applies to functions *in the plane*. In fact, let $\delta_{(x_0, y_0)}(x, y)$ be defined by the integral

$$\int_{-\infty}^{\infty} \int_{-\infty}^{\infty} f(x, y) \delta_{(x_0, y_0)}(x, y) dx dy = f(x_0, y_0)$$

for all continuous $f(x, y)$. Let $\delta_0 = \delta_{(0,0)}$ denote the delta function at the origin. In polar coordinates, and for radial functions $f = f(r)$, δ_0 has the property

$$\int_0^{\infty} \int_0^{2\pi} f(r) \delta_0(r, \theta) r dr d\theta = f(0),$$

which simplifies to

$$\int_0^{\infty} f(r) \delta_0(r) r dr = \frac{f(0)}{2\pi} \quad (42)$$

because δ_0 is independent of θ . Thus

$$\bar{\delta}_0(\kappa) = \int_0^{\infty} \delta_0(r) J_0(\kappa r) r dr = \frac{J_0(0)}{2\pi} = \frac{1}{2\pi}.$$

APPENDIX B. THE DISC LOAD CASE

As an exercise and for verification purposes we describe a solution to the viscous half-space flat earth equation (2). The inverse Hankel transform of this solution is a solution to equation (17).

Consider a disc load centered at the map-plane origin, of radius R_0 and thickness H_0 . In this case

$$\sigma_{zz}(r) = \begin{cases} -\rho_i g H_0, & 0 < r < R_0, \\ 0, & R_0 < r \end{cases}$$

where ρ_i is the density of the load; we might as well suppose it is ice. Actually, let's suppose this load is applied at time zero and is held in place: $\sigma_{zz}(r, t) = \sigma_{zz}(r)H(t)$. Because this load is radial, the Hankel-transformed equation (2) is useful. We will assume an undeformed state $\bar{u}^V = 0$ at time $t = 0$.

We need the Hankel transform $\bar{\sigma}_{zz}$:

$$\bar{\sigma}_{zz}(\kappa) = -\rho_i g H_0 \int_0^{R_0} J_0(\kappa r) r dr = -\frac{\rho_i g H_0}{\kappa^2} \int_0^{\kappa R_0} J_0(s) s ds = -\rho_i g H_0 R_0 \kappa^{-1} J_1(\kappa R_0),$$

using the change-of-variable $s = \kappa r$ and the identity $\frac{d}{ds}(sJ_1(s)) = sJ_0(s)$ (formula (8) in Appendix A of (Sneddon 1951)).

Now, we can solve (2) because it is simply a collection of decoupled first-order linear ODE problems in time:

$$\bar{u}^V(\kappa, t) = \rho_i g H_0 R_0 \frac{\{\exp(-\beta(\kappa)t/(2\eta\kappa)) - 1\} J_1(\kappa R_0)}{\kappa \beta(\kappa)}$$

for $t > 0$ and $\bar{u}^V(\kappa, t) = 0$ for $t \leq 0$, where $\beta(\kappa) = \rho_r g + D\kappa^4$. The displacement can be found by an (inverse) Hankel transform

$$u^V(r, t) = \rho_i g H_0 R_0 \int_0^\infty \beta(\kappa)^{-1} \{ \exp(-\beta(\kappa)t/(2\eta\kappa)) - 1 \} J_1(\kappa R_0) J_0(\kappa r) d\kappa. \quad (43)$$

This integral can be computed numerically, but care must be taken because the integrand is quite oscillatory. We break up the integrand into many (≥ 100) subintervals and call MATLAB's `quadl` on each subinterval. The code `viscdisc` in Appendix D implements equation (43). In particular, we believe that computing (43) for geophysically reasonable parameter values is quite accurate, and that the result can be used to verify the result from the Fourier spectral collocation method described in section 3. See section 5 for results. The displacement for a particular disc load is graphed in figure 16. This solution looks rather like the Green's function G^V plotted in figure 2, as expected, but with a wider depressed area.

The equilibrium limit of this disc load solution is of interest:

$$u^\infty(r) = \lim_{t \rightarrow \infty} u^V(r, t) = -\rho_i g H_0 R_0 \int_0^\infty \beta(\kappa)^{-1} J_1(\kappa R_0) J_0(\kappa r) d\kappa. \quad (44)$$

This function satisfies the PDE $\rho_r g u^\infty + D\Delta^2 u^\infty = \sigma_{zz}$. It appears in figure 16, and we see the peripheral “dip” and “bulge” which occur at the edge of the disc. Note that the central part of disc load of thickness H_0 and large radius descends to the “compensation depth” $-(\rho_i/\rho_r)H_0$.

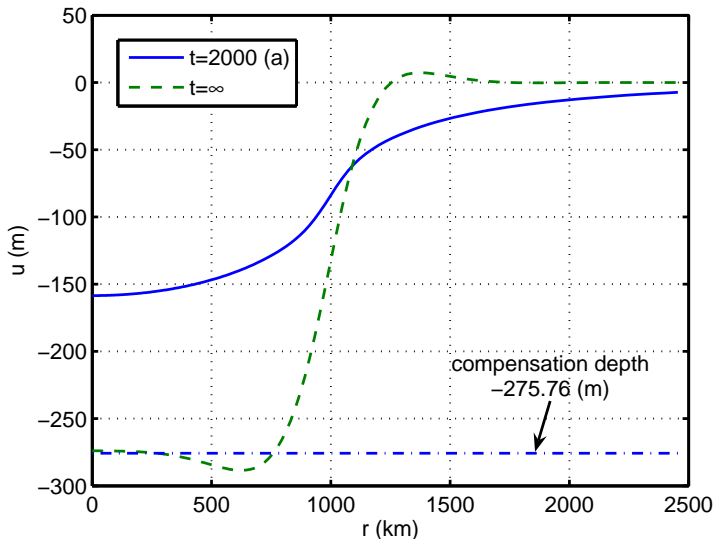


FIGURE 16. Vertical displacement at 2000 years, and the equilibrium position at time ∞ , for a disc load of ice with thickness 1000 (m) and radius 1000 (km). “Compensation depth” corresponding to $\rho_i = 910$, $\rho_r = 3300$ (kg m^{-3}) also shown. Note log scale on horizontal axis.

APPENDIX C. ON “GREEN’S FUNCTION THINKING” FOR PDE (17)

Here we make some comments on formula (6) in section 1 which relate it to results in section 3. The time integral in (6) starts from $-\infty$ to avoid requiring precise knowledge

of the displacement $u^V(x, y, t_0)$ at any particular past time t_0 . That is, (6) computes the displacement at time t caused by a load history known so far into the past that prior displacement states are irrelevant. This is reasonable because the underlying PDE, equation (17) in section 3, is diffusive and thus the influence of any displacement state decays exponentially in time.

If, on the other hand, an initial displacement $u(x, y, t_0)$ is known at a relatively recent past time then we must adjust (6). As a start, integrating (6) by-parts in the time variable and assuming $\Psi(x, y, -\infty)$ is zero gives the formula

$$u^V(x, y, t) = \int_{-\infty}^t \iint_R \frac{\partial G^V}{\partial t}(|\mathbf{r} - \mathbf{r}'|, t - t') \Psi(x', y', t') dx' dy' dt'. \quad (45)$$

Our assumption that there is no load at $t = -\infty$ is equivalent to assuming $\Psi(x, y, t) = \int_{-\infty}^t \lambda(x, y, s) ds$. The significance of (45) is that the load function Ψ reappears and that we are motivated to examine $\partial G^v / \partial t$.

From (5) note that

$$\frac{\partial G^V}{\partial t}(r, t) = -\frac{g}{2\pi} \int_0^\infty (2\eta\kappa)^{-1} \exp[-\beta(\kappa)t/(2\eta\kappa)] J_0(\kappa r) \kappa d\kappa. \quad (46)$$

In fact, formula (46) can also be extracted from equation (20) in section 3:

$$\begin{aligned} \frac{\partial G^V}{\partial t}(x, y, t) &= -\frac{g}{2\pi} \mathcal{F}_2^{-1} \left\{ \frac{\exp[-\beta(\xi, \zeta)t/(2\eta(\xi^2 + \zeta^2)^{1/2})]}{2\eta(\xi^2 + \zeta^2)^{1/2}} \right\} \\ &= -\frac{g}{2\pi} \int_0^\infty (2\eta\kappa)^{-1} \exp[-\beta(\kappa)t/(2\eta\kappa)] J_0(\sqrt{x^2 + y^2} \kappa) \kappa d\kappa. \end{aligned} \quad (47)$$

Here \mathcal{F}_2 stands for the two-variable Fourier transform and $\beta(\kappa) = \rho_r g + D\kappa^4$ as in section 1. The second equality in (47) is explained by noting (Appendix A) that \mathcal{F}_2 becomes the Hankel transform on radial functions. Comparing to section 1, $\sigma_{zz}(x, y, t) = -g\Psi(x, y, t)$ (N m^{-2}) if Ψ (kg m^{-3}) is the load function.

Returning now to equation (45), we can see from (20) how to modify (45) to include knowledge of displacement at a finite time t_0 . In fact, the convolution theorem

$$\mathcal{F}_2^{-1} \{ \tilde{f} \tilde{g} \} = \frac{1}{2\pi} (f * g) = \frac{1}{2\pi} \iint_{\mathbb{R}^2} f(x - x', y - y') g(x', y') dx' dy'$$

now allows us to write the inverse Fourier transform of (20) as

$$\begin{aligned} u^V(x, y, t) &= \int_{t_0}^t \iint_{\mathbb{R}^2} \frac{\partial G^V}{\partial t}(|\mathbf{r} - \mathbf{r}'|, t - s) \Psi(x', y', s) dx' dy' ds \\ &\quad + \iint_{\mathbb{R}^2} \gamma(|\mathbf{r} - \mathbf{r}'|, t - t_0) u(x', y', t_0) dx' dy' \end{aligned} \quad (48)$$

where

$$\gamma(r, t) = \frac{1}{2\pi} \int_0^\infty \exp[-\beta(\kappa)t/(2\eta\kappa)] J_0(r\kappa) \kappa d\kappa.$$

In our view equation (48) proves equation (6). We have justified the heuristic Green's function thinking in section 1 by a standard linear analysis of PDE (17). Note that as $t \rightarrow \infty$, $\gamma(r, t) \rightarrow 0$. Thus as $t_0 \rightarrow -\infty$ the last term in (48) disappears. The decaying

kernel γ describes the rate at which information held in the previous displacement $u(x, y, t_0)$ is eliminated.

APPENDIX D. MATLAB CODES

This section gives MATLAB implementations of the numerical strategies outlined in sections 2, 3, and Appendix B. Here is a synopsis of the three codes:

- **geforconv** precomputes the spherical elastic load response matrix I^E , given by equation (9), which is the computational form of the Green's function G^E . It numerically computes integrals (9) by using MATLAB's `dblquad` with the default settings, where the integrand comes from linearly interpolating the tabular data given by (Farrell 1972). If **geforconv** has been run on the given grid, **fastearth** (below) then convolves I^E with the load, as noted, using MATLAB's `conv2` for now because it seems sufficiently fast; an FFT-based alternative is reasonable. The precomputation is much more expensive than running the viscous deformation model or convolving I^E with the load. For instance, in the MATLAB run

```
tic, I = geforconv(256,256,2000,2000); toc
save I256 I
tic, fastearth(256,100000,500,4,'testC'); toc
```

the call to **geforconv** requires about 4 *hours* while only 10 *minutes* is required to run **fastearth**; the machine is a 3 GHz Pentium IV.

- **fastearth** computes the viscous model using `fft2` to compute equation (26). It also convolves I^E with the load for the spherical elastic model as noted. In this example implementation the load is either a standard disc load or a modification to Test C from (Bueler et al. 2005).
- **viscdisc** implements formula (43) in Appendix B.

geforconv.m:

```
function II=geforconv(Nx,Ny,Lx,Ly);
% GEFORCONV Computes matrix I=I(p,q), a form of the elastic "load response
% matrix" described in Lingle & Clark (1985) and in the technical report
% Bueler (2005). Matrix I(p,q) is used by FASTEARTH.
%
% I=GEFORCONV(NX,NY,LX,LY) computes (2 NX + 1) by (2 NY + 1)
% matrix I with entries
% /dy/2 /dx/2
% I(p,q)= | | G^E(sqrt((pdx-xi)^2+(qdy+eta^2))) dxi deta
% /-dy/2 /-dx/2
% where dx=2 LX/NX, dy=2 LY/NY. Input LX,LY in km. Assumes region
% extends from x=-LX to x=LX and y=-LY to y=LY. Uses Matlab's
% dblquad to do integral.
%
% Example:
% I=geforconv(16,16,2000,2000);
%
% See also FASTEARTH.
% ELB 12/11/05.

rm=[ 0.011 0.111 1.112 2.224 3.336 4.448 6.672 8.896 11.12 17.79 ...
```

```

    22.24 27.80 33.36 44.48 55.60 66.72 88.96 111.2 133.4 177.9 ...
    222.4 278.0 333.6 444.8 556.0 667.2 778.4 889.6 1001.0 1112.0 ...
    1334.0 1779.0 2224.0 2780.0 3336.0 4448.0 5560.0 6672.0 7784.0 8896.0 ...
    10008.0] * 1e3; % converted to meters
% GE /(10^12 rm) is vertical displacement in meters
GE=[-33.64 -33.56 -32.75 -31.86 -30.98 -30.12 -28.44 -26.87 -25.41 ...
    -21.80 -20.02 -18.36 -17.18 -15.71 -14.91 -14.41 -13.69 -13.01 ...
    -12.31 -10.95 -9.757 -8.519 -7.533 -6.131 -5.237 -4.660 -4.272 ...
    -3.999 -3.798 -3.640 -3.392 -2.999 -2.619 -2.103 -1.530 -0.292 ...
    0.848 1.676 2.083 2.057 1.643];
% linearly extrapolate GE to r=0; GE(0) := -33.6488
GE=[interp1(rm(1:2),GE(1:2),0.0,'linear','extrap') GE];
rm=[0.0 rm]; % length(rm)=length(GE)=42

dx=2*Lx*1000/Nx; dy=2*Ly*1000/Ny; % dimensions of load element
II=zeros(2*Nx-1,2*Ny-1);
% compute entries of II by dblquad, using quad method and default TOL=1e-6
for p=-Nx+1:Nx-1
    for q=-Ny+1:Ny-1
        II(p+Nx,q+Ny)=dblquad(@integrand,-dx/2,dx/2,-dy/2,dy/2);
    end
end

% nested function which is integrand in I(p,q)
function z=integrand(xi,eta)
    r=sqrt((p*dx-xi).^2+(q*dy-eta).^2);
    z=zeros(length(r));
    for jj=1:length(r)
        if r(jj)==0.0 % treat normalization r as 11 m
            z(jj)=GE(1)/(rm(2)*1e12);
        elseif r(jj)>=rm(end), z(jj)=0;
        else % linearly interpolate to get GE value; then normalize
            ii=find(rm>r(jj),1); % 2 <= ii <= 42
            z(jj)=interp1(rm(ii-1:ii),GE(ii-1:ii),r(jj))/(r(jj)*1e12);
        end
    end
end

end
end

end

```

fastearth.m:

```

function [uv,ue,H,xs,ys]=fastearth(Nin,tf,dtyear,Z,type,graphflag)
% FASTEARTH Use the elastic-viscous earth model from
% Bueler (2006) "Computation of a viscoelastic deformable earth
% model for ice sheet simulation."
% to simulate the deformation of the earth under a disc load or under an
% artificial ice sheet load history. Uses a modified "load response
% matrix" approach for the elastic component. Uses a Fourier spectral
% method (Trefethen 2000) for the flat-earth, elastic plate over viscous
% half-space model. The PDE for this latter model is
% d/dt(2 eta Lap^{1/2} u) + rho g u + D Lap^2 u = sigma_zz.
% Time discretization of this PDE is Crank-Nicolson. The source of the
% model is
% Lingle & Clark (1985) "A numerical model of interactions between a
% marine ice sheet and the solid earth: Application to a West Antarctic
% ice stream," J. Geophysical Research 90 (C1) 1100--1114.

```



```

%
% [UV,UE,HH,XX,YY]=FASTEARTH(N,TF,DTYEAR,Z) computes and plots
% deformation of the earth's surface under an ice disc load of radius
% 1000km and thickness 1000m. Uses N grid points in each direction on
% a square 4000 km by 4000 km region R of physical interest. N must be
% even; best choices are powers of 2. Z is a small whole number
% (Z=2 recommended) which determines the size of the computational
% region Omega for the flat viscous model. Namely, Omega is a square
% with side 4000*Z km, discretized by N*Z points in each direction. A
% periodic boundary condition is applied at the edge of Omega. TF is
% # of years of the run with timestep DTYEAR. Elastic deformation is
% performed on R and is only done if a file "I{N}.mat" can be found;
% this can be generated using GEFORCONV; see examples. FASTEARTH
% returns the gridded flat viscous deformation UV, the gridded elastic
% deformation UE, the thickness HH--all at the final time---and the
% grid itself in XX,YY (as from MESHGRID); all outputs in meters.
%
% [UV,UE,HH,XX,YY]=FASTEARTH(N,TF,DTYEAR,Z,'disc') Same as above.
%
% [UV,UE,HH,XX,YY]=FASTEARTH(N,TF,DTYEAR,Z,'testC') is the same except
% that the ice load is essentially test C, but with simple isostacy
% added, from
%
%   Bueler, et al. (2005) "Exact solutions and the verification of
%   numerical models for isothermal ice sheets," J. Glaciol. 51 (173)
%   291--306.
%
% Thickness evolution is stopped at 40033 years and the last thickness
% held.
%
% [UV,UE,HH,XX,YY]=FASTEARTH(N,TF,DTYEAR,Z,'...',false) No graphing.
%
% Example I; generate I for 16 x 16 case, store and use:
%   tic, I = geforconv(16,16,2000,2000); toc % about a minute
%   save 'I16' I
%   fastearth(16,100000,500,2); % 2 secs
% Example II; to see ice cap on bed; needs "I128.mat":
%   [uv,ue,H,x,y]=fastearth(128,40000,500,2,'testC'); % 15 secs
%   figure, mesh(x/1000,y/1000,H+uv+ue)
%   hold on, mesh(x/1000,y/1000,uv+ue), hold off
% See also GEFORCONV, VISCDISC, TESTFAST.
% ELB 1/12/06

if nargin<5, Cflag=false; type='disc'; end
if nargin<6, graphflag=true; end
if strcmp(type,'testC'), Cflag=true;
else, Cflag=false; end
if ((floor(Z)~=ceil(Z)) || (Z<1)), error('Z must be positive integer'), end

g=9.81; spera=3.1556926e7; % seconds per year
rhoi=0.910e3; % density of ice; kg/m^3
rhor=3.300e3; % density of mantle; kg/m^3
D=5.0e24; % flexural rigidity of lithosphere as an elastic plate
eta=1.0e21; % viscosity of mantle

L0=2000e3; % half-length of actual domain in each direction; m

% compute flat-earth, viscous half-space model on extended grid:
L=Z*2000e3; % half-length of computational domain
N=Z*Nin; % computational N

```

```

h=2*L/N;  x=-L+h:h:L;
[xx,yy]=meshgrid(x,x);  rr=sqrt(xx.^2+yy.^2);
M=ceil(tf/dtyear);  dt=(tf/M)*spera;

% Fourier coefficients of powers of Laplacian
cx=(pi/L)*[0:N/2 N/2-1:-1:1];
[ccxx,ccyy]=meshgrid(cx,cx);
cclap=ccxx.^2+ccyy.^2;
cchalf=sqrt(cclap);  % lap^{1/2} coeffs
ccbih=cclap.^2;  % biharmonic coeffs

% coefficients in transformed PDE
part1=2*eta*cchalf;
part2=(dt/2)*( rhor*g*ones(size(ccbih)) + D*ccbih );
right = part1 - part2;  % Fourier-transformed operator on right of eqn (19)
left = part1 + part2;  % ... on left of eqn

disp(' computing flat viscous deformation ...')
uun1=zeros(size(xx));
for n=0:M-1
    uun=uun1;
    if Cflag, H=getTestC(xx,yy,(n+1/2)*dt);
    else, H=1000*(rr<1e6); end
    % apply Fourier spectral method:
    sssz=-rhoi*g*H;
    frhs=right.*fft2(uun) + fft2(dt*sssz);
    uun1=real(ifft2( frhs./left ));
end
% tweak: find average value along "distant" bdry of [-ZL,ZL]X[-ZL,ZL],
% remove it and add back result for equivalent disc load
uun1=uun1-( sum(uun1(1,:))+sum(uun1(:,1)) )/(2*N);
if Cflag % assume equiv disc load has R0=1000km
    HO=h*h*sum(sum(H))/(pi*1e6^2); % trapezoid rule
else, HO=1000; end
uun1=uun1+viscdisc(HO,1000,tf,L/1000);

sh=(N/2)-(N/(2*Z))+1:(N/2)+(N/(2*Z)); % extract central/actual part
xs=xx(sh,sh);  ys=yy(sh,sh);  uv=uun1(sh,sh);  H=H(sh,sh);

% get and use (w. convolution) elastic LRM if available; plot things
filename=['I' num2str(Nin) '.mat'];
doGE=(exist(filename)==2);
if doGE, disp(' [elastic load response matrix FOUND]')
else, disp(' [elastic load response matrix NOT found]'), end
if doGE
    disp([' computing spherical elastic deformation using I' ...
        num2str(Nin) '.mat ...'])
    S=load(filename);
    ue=rhoi*conv2(H,S,I,'same');
    if graphflag
        figure(1), clf, subplot(2,1,2), mesh(xs/1000,ys/1000,ue);
        xlabel('x (km)'), ylabel('y (km)')
        zlabel('vertical displacement (m)')
        title('spherical, self-gravitating elastic model')
        subplot(2,1,1), mesh(xs/1000,ys/1000,uv);
    end
end
else
    disp(' skipping spherical elastic deformation ...')
end

```

```

    ue=zeros(size(uv)); % for return value only
    if graphflag, figure(1), clf, mesh(xs/1000,ys/1000,uv); end
end
if graphflag
    xlabel('x (km)'), ylabel('y (km)')
    zlabel('vertical displacement (m)')
    title('elastic plate over viscous half-space model')
end

function H=getTestC(x,y,t)
% compute exact H from test C (with simple isostasy added) in Bueller et al
% "Exact solutions ... isothermal ice sheets". Stops growth at time
% t0=40033 years.
spera=3.1556926e7; % seconds per year
H0=3600; R0=750000;
% see "Exact solutions ..." eqn (9):
% t0=(2/9.0177e-13)*(7/((1-(910/3300))*4))^3*(R0^4/H0^7) is 40034 years
t0=40034*spera;
ts=t/t0; if ts>1, ts=1.0; end
rscl=(ts^(-2))*(sqrt(x.^2+y.^2)/R0);
H=H0*ts*max(0, 1-rscl.^(4/3)).^(3/7);

```

viscdisc.m:

```

function u=viscdisc(H0,R0km,tyrs,rkm)
% VISCDISC Solution of viscous half-space overlain by rigid lithosphere in
% case of disc load at origin. Computed by Hankel transform means for
% comparison to Lingle & Clark (1985) and to new numerical method in
% technical report: Bueller (2005), "Computation of a viscoelastic
% deformable earth model for ice sheet simulation."
%
% [R,U]=VISCDISC(H0,R0KM,TYRS,RKM) computes the displacement U at
% time TYRS (years) at radii RKM (km) caused by a disc of radius
% R0KM (km) and thickness H0 (m). RKM may be a vector; U will be a
% vector of the same length.
%
% [R,U]=VISCDISC(H0,R0KM,'INF',RKM) computes the equilibrium
% displacement.
%
% Example I; for disc 1000 m thick with 1000km radius at t=10^2,10^4,inf
% years; plotted on range 0.01 km to 10000 km. Each evaluation of
% viscdisc requires more than a minute on my machine.
%
% r=10.^(-2:.01:4); % 601 r values
% u1=viscdisc(1000,1000,100,r);
% u2=viscdisc(1000,1000,2000,r);
% u3=viscdisc(1000,1000,'inf',r);
% semilogx(r,u1,r,u2,r,u3), xlabel('r (km)'), ylabel('u (m)')
% u3(1)/1000, -910/3300 % compensation depth comparison
%
% Example II; continues the above. Plots the Green's function as in figure
% 5(a) in Lingle & Clark (1985), but at fewer times. Takes a minute or so.
%
% tt=[20 200 500 2000 5000 20000 50000 100000];
% R0=0.001; H0=1/(pi*910); % small disc with mass 1 kg
% for j=1:8, uu(:,j)=viscdisc(H0,0.001,tt(j),r); end
% figure, for j=1:8, semilogx(r,uu(:,j)), hold on, end

```

```

% hold off, xlabel('r (km)'), ylabel('displacement (m)')
% axis([r(1) r(end) -3.5e-15 0.5e-15]), grid on
%
% See also GHV, FASTEARTH, TESTFAST.
% ELB (12/7/05)

g=9.81; % m/s^2
rhoi=910; % kg/m^3
rhor=3300; % kg/m^3
rg=rhor*g; % combined constant
D=5.0e24; % N m; flexural rigidity of lithosphere
eta=1.0e21; % Pa s; viscosity of mantle
spera=3.1556926e7; % seconds per year

R0=R0km*1000;
TOL=eps;
pts=[10.^(-3:-0.05:-10) 1.0e-14];

if (isstr(tyrs)&&strcmp(tyrs,'inf'))
    for k=1:length(rkm)
        rk=rkm(k)*1000;
        result=quadr(@equilgrand,pts(1),100.0*pts(1),TOL); %kap->infy tail
        for j=1:length(pts)-1
            result=result+quadr(@equilgrand,pts(j+1),pts(j),TOL);
        end
        u(k)=-rhoi*g*H0*R0*result;
    end
else
    t=tyrs*spera;
    for k=1:length(rkm)
        rk=rkm(k)*1000;
        result=quadr(@integrand,pts(1),100.0*pts(1),TOL); % kap->infy tail
        for j=1:length(pts)-1
            result=result+quadr(@integrand,pts(j+1),pts(j),TOL);
        end
        u(k)=rhoi*g*H0*R0*result;
    end
end

function y=integrand(kap)
% integrand of inverse Hankel transform
beta=rg + D*kap.^4;
expdiff=exp(-beta*t./(2*eta*kap))-ones(size(kap));
y=expdiff.*besselj(1.0,kap*R0).*besselj(0.0,kap*rk)./beta;
end

function y=equilgrand(kap)
% integrand of inverse Hankel transform when t-->infy
y=besselj(1.0,kap*R0).*besselj(0.0,kap*rk)./(rg + D*kap.^4);
end

end

```
